GEODYNAMICS & TECTONOPHYSICS
Published by the Institute of the Earth's Crust, Siberian Branch, Russian Academy of Sciences

PALEOGEODYNAMICS

2022 VOLUME 13 ISSUE 3 ARTICLE 0637

ISSN 2078-502X

DOI: 10.5800/GT-2022-13-3-0637

LATE PALEOZOIC CONTRASTING MAGMATISM OF THE EASTERN KAAKHEM MAGMATIC AREA (CENTRAL ASIAN OROGENIC BELT)

I.V. Karmysheva [1]✉, **V.A. Yakovlev** [1], **A.M. Sugorakova** [2], **S.N. Rudnev** [1], **D.V. Semenova** [1]

[1] Sobolev Institute of Geology and Mineralogy, Siberian Branch of the Russian Academy of Sciences, 3 Academician Koptyug Ave, Novosibirsk 630090, Russia

[2] Tuvinian Institute for Exploration of Natural Resources, Siberian Branch of the Russian Academy of Sciences, Internatsionalnaya St, 117a, Kyzyl, 667007, Republic of Tyva, Russia

ABSTRACT. Based on the isotope-geochronological (zircons, U-Pb method), petrogeochemical, and structural and petrologic data, the following paper provides a detailed description of the characteristics of the Late Paleozoic basic and granitoid magmatism in the eastern part of the Kaakhem magmatic area (Eastern Tuva). During the formation of the Shivey alkaline-granitoid and Chadal gabbroid massifs in the period of 292–283 Ma, there were revealed two stages of contrasting magmatism. The early stage is characterized by the formation of plutonic mingling structures and intermediate rocks. Deformation structures, widespread in the early-mingling rocks, are superimposed and formed in extensional regime. At a later stage, there occurred a sequential intrusion of salic and mafic magmas into the zones of local extension in the early-mingling host rocks. A similar petrogeochemical composition of basic rocks of the early and late mingling indicates that they all formed from enriched magma. Granosyenites and granites are derived from melting of tonalites and metasedimentary rocks with a significant contribution of the mantle component. The simultaneous formation of the Chadal gabbroid and Shivei granitoid massifs took place at the intraplate stage of the development of geological structures of Eastern Tuva in the Late Paleozoic.

KEYWORDS: Early Permian magmatism; gabbro-granite magmatism; mingling; U-Pb method; Kaakhem batolith

FUNDING: Work is done on state assignment of IGM SB RAS.

RESEARCH ARTICLE

Received: August 24, 2021
Revised: December 27, 2021
Accepted: January 11, 2022

Correspondence: Irina V. Karmysheva, iri@igm.nsc.ru

FOR CITATION: Karmysheva I.V., Yakovlev V.A., Sugorakova A.M., Rudnev S.N., Semenova D.V., 2022. Late Paleozoic Contrasting Magmatism of the Eastern Kaakhem Magmatic Area (Central Asian Orogenic Belt). Geodynamics & Tectonophysics 13 (3), 0637. doi:10.5800/GT-2022-13-3-0637

ПОЗДНЕПАЛЕОЗОЙСКИЙ КОНТРАСТНЫЙ МАГМАТИЗМ ВОСТОЧНОЙ ЧАСТИ КААХЕМСКОГО МАГМАТИЧЕСКОГО АРЕАЛА (ЦЕНТРАЛЬНО-АЗИАТСКИЙ СКЛАДЧАТЫЙ ПОЯС)

И.В. Кармышева[1], В.А. Яковлев[1], А.М. Сугоракова[2], С.Н. Руднев[1], Д.В. Семенова[1]

[1] Институт геологии и минералогии им. В.С. Соболева СО РАН, 630090, Новосибирск, пр-т Академика Коптюга, 3, Россия

[2] Тувинский институт комплексного освоения природных ресурсов СО РАН, 667007, Кызыл, ул. Интернациональная, 117а, Республика Тыва, Россия

АННОТАЦИЯ. В настоящей работе на основе изотопно-геохронологических (цирконы, U-Pb метод), петрогеохимических и структурно-петрологических данных приводится характеристика позднепалеозойского магматизма Каахемского ареала (Восточная Тува). Выявлены два этапа контрастного по составу магматизма при становлении Шивейского щелочно-гранитоидного и Чадалского габброидного массивов в период 292–283 млн лет. Ранний этап характеризуется формированием структур плутонического минглинга и образованием пород промежуточного состава. Деформационные структуры, широко распространенные в породах раннего минглинга, имеют наложенный характер и формировались в обстановках растяжения. На позднем этапе последовательное внедрение салических и мафических магм происходило в зоны локального растяжения во вмещающих породах раннего минглинга. Мафические породы раннего и позднего минглинга идентичны по петрогеохимическому составу, что указывает на их происхождение из единого глубинного обогащенного источника. Образование граносиенитов и гранитов связано с плавлением тоналитов и метаосадочных пород со значительным вкладом мантийного компонента. Одновременное становление Чадалского габброидного и Шивейского гранитоидного массивов происходило на внутриплитном этапе развития геологических структур Восточной Тувы в позднем палеозое.

КЛЮЧЕВЫЕ СЛОВА: раннепермский магматизм; габбро-гранитный магматизм; минглинг; U-Pb метод; Каахемский батолит

ФИНАНСИРОВАНИЕ: Исследование выполнено по государственному заданию ИГМ СО РАН.

1. INTRODUCTION

The magmatic complexes within the Central Asian Orogenic Belt (CAOB) were formed from the Late Proterozoic to Mesozoic geodynamic settings. The Late Paleozoic magmatism is associated with the formation of large-volume granitoid intrusions (Angara-Vitim, Khangai, Kalba-Narym batholiths) and is the largest-scale in the CAOB [Dobretsov et al., 2010; Xiao et al., 2010; Yarmolyuk et al., 2013; Tsygankov, 2014; and others]. Many authors relate the Late Paleozoic–Early Mesozoic magmatism to intraplate rifting structures and emphasize its spatiotemporal relationship with the enriched mantle-derived magmas [Yarmolyuk et al., 2000; Yarmolyuk, Kovalenko, 2003; Vladimirov et al., 2008; Kuz'min et al., 2011; Yarmolyuk, Kuzmin, 2011; Yarmolyuk et al., 2013; Kozlovsky et al., 2015; and others].

The Kaakhem magmatic area (~30000 km^2), which is the object of this paper, relates to the structures of eastern Tuva and is one of the largest magmatic formations of the Altai-Sayan folded area (Fig. 1). The area formation is related to the stages of Early Paleozoic and Late Paleozoic magmatism. The early-stage granitoids (Fig. 1) have a wide-area distribution and are thoroughly studied [Rudnev et al., 2015; Sugorakova, Khertek, 2017].

The Late Paleozoic magmatism, however, has local manifestations insufficiently explored thus far (spatially converging Shivey granosyenite-granite and Chadal gabbroid massifs) [Sugorakova, 2017]. The questions are still unanswered with regard to petrogenesis of granitoids, tectonic settings of magmatism, and relationship between basite and granitoid magmatism.

This paper aims to provide a description of the Late Paleozoic stage of formation of the Kaakhem magmatic area on the basis of isotope chronology and structural petrology data.

2. GEOLOGICAL POSITION

The Shivey massif occupies an area of about 500 km^2 and is mostly located on the left bank of the Kaa-Khem River along the Shivey River (Fig. 1). The Chadal gabbroid massif (4×3 km) is located in the northern Shivey massif on the right bank of the Kaa-Khem River (Fig. 2). The massif which was earlier considered as a part of bimodal association of the Shivey massif [Sugorakova et al., 2011] was

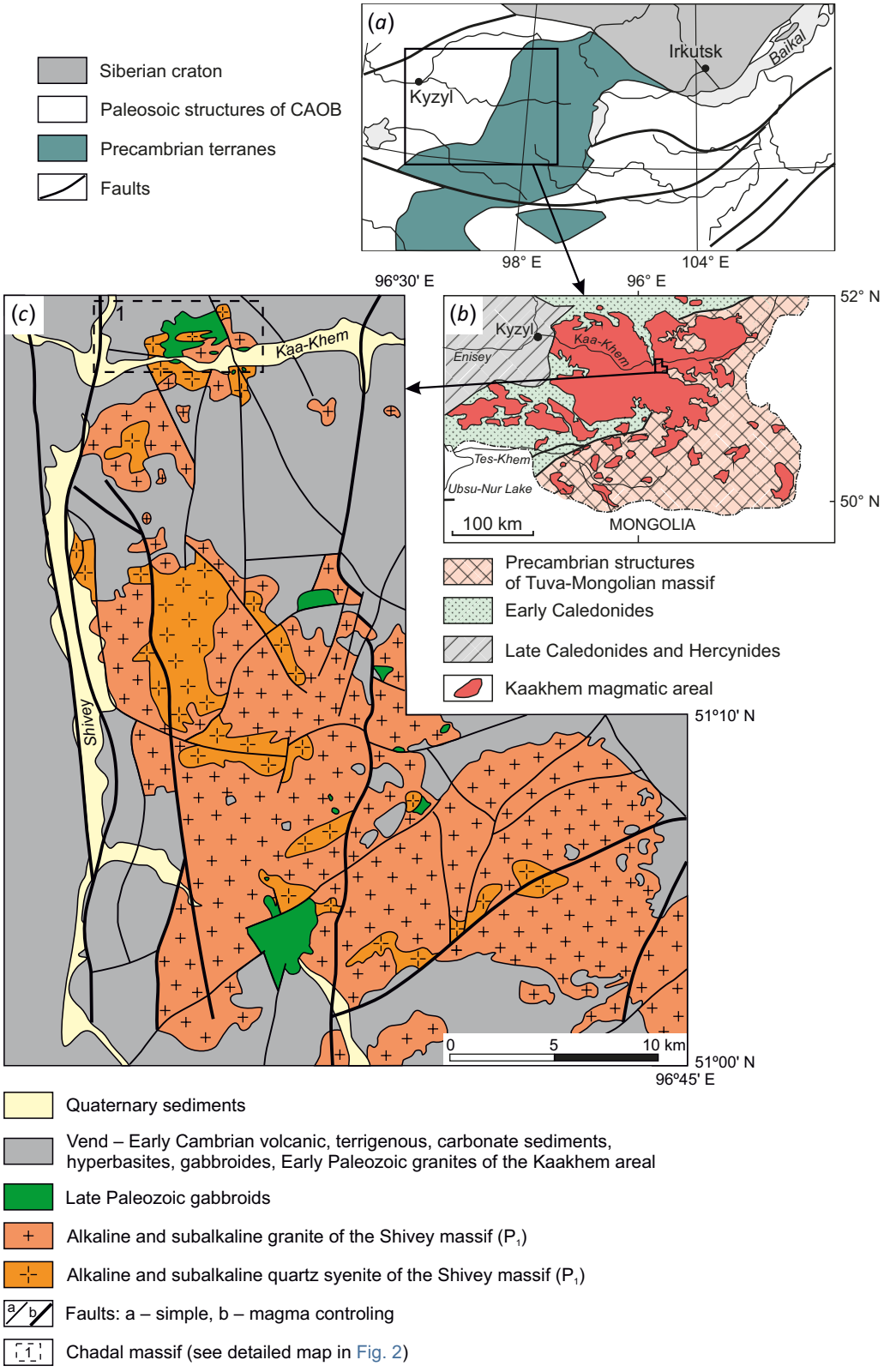

Fig. 1. Location of the Shivei massif in the structures of the Central Asian fold belt.
(*a*) – location of the Kaakhem areal in the structures of the southern frame of the Siberian Craton (after [Kuzmichev, 2004]); (*b*) – location of the Shivey massif in the Kaakhem areal modified (after [Rudnev et al., 2015]); (*c*) – scheme of the geological structure of the Shivey massif [Sugorakova et al., 2011].

Рис. 1. Расположение Шивейского массива в структурах Центрально-Азиатского складчатого пояса.
(*a*) – положение Каахемского ареала в структурах южного обрамления Сибирской платформы (по [Kuzmichev, 2004], с упрощениями); (*b*) – положение Шивейского массива в Каахемском ареале (по [Rudnev et al., 2015], с упрощениями); (*c*) – схема геологического строения Шивейского массива [Sugorakova et al., 2011].

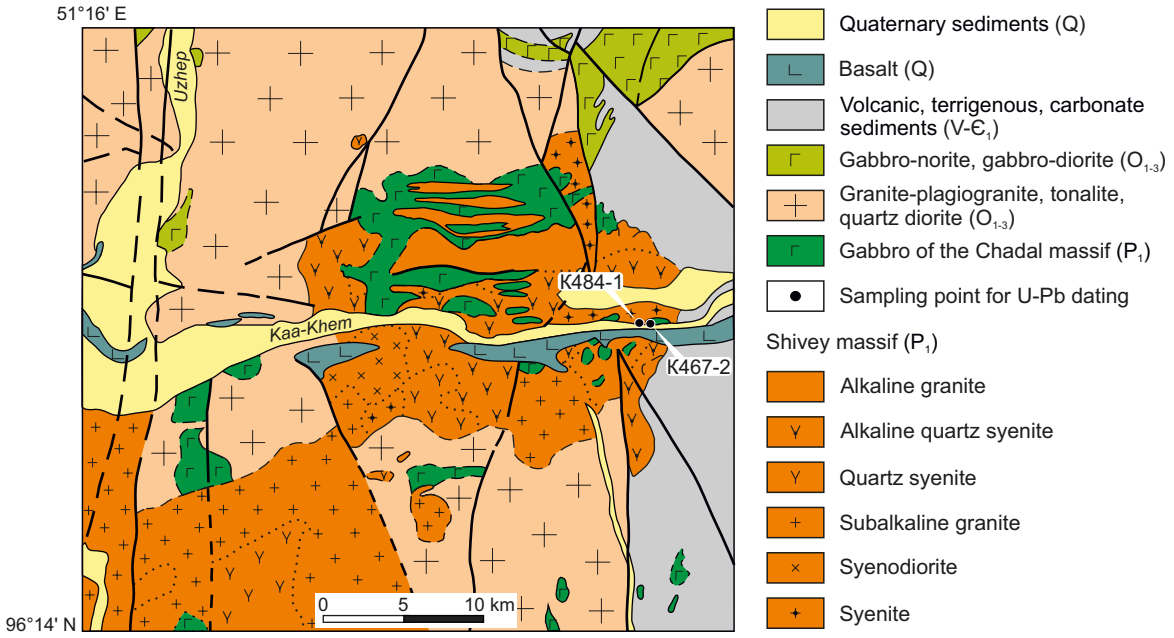

Fig. 2. Geological map of the Shivey and Chadal massifs structure (a fragment of the State Geological Map, scale 1:50000, 1990. Responsible executor – A.M. Sugorakova).

Рис. 2. Геологическая карта строения Шивейского и Чадалского массивов (фрагмент Государственной геологической карты масштаба 1:50000, 1990. Ответственный съемщик – Сугоракова А.М.).

first defined to be a separate structure and described in [Sugorakova, 2017].

The Shivey massif is composed of syenites, syenodiorites, quartz syenites, granosyenites, and granites. Ill-defined contact varieties exhibit gradual transition from one rock type to another through increasing or decreasing this or that mineral content. The varieties characterized by constant mineral content comprise the areas of 10 cm^2 to a few tens and hundreds of square meters. The massif rocks are arranged irregularly, the boundaries drawn on the map are conditional, and the rocks are designated in accordance with the predominant type. The Shivey massif rocks are further named granosyenites and granites, except for the moments when the precise name of the rock is of principal importance. U-Pb dating of zircons from alkaline-rich quartz syenites and alkaline-rich granodiorites (SHRIMP-II, Saint-Petersburg) yielded the ages of 297±4 and 293±4 Ma, respectively [Sugorakova et al., 2011].

The Chadal massif is composed of amphibole gabbro, monzogabbro, diorites, and monzodiorites. There are no well-defined contact varieties. The massif rocks do not show any distribution pattern. The massif rocks are further named monzogabbro in accordance with the average composition of rocks.

3. RESEARCH TECHNIQUE

The magmatic rock studies involve the methods of structural petrology, determining the petrogeochemical composition of rocks, and U-Pb dating.

The studies of rock composition were performed at the Center for Isotope-Geochemical Investigations, Institute of Geochemistry SB RAS (the city of Novosibirsk) (determination of petrogenic elements by XRF analysis and that of rare-earth and high-field strength elements by ICP-MS), Analytical Center for Geochemistry of Natural Systems at the GGF TSU (the city of Tomsk) (determination of rare-earth and high-field strength elements by ICP-MS), and the Center for Isotope-Geochemical Investigations IG SB RAS (petrochemical studies by XRF analysis) (the city of Irkutsk).

U-Pb geochronology of zircons was performed at the Center for Multielement and Isotope Analysis IGM SB RAS (the city of Novosibursk) via LA-SF-ICP-MS using the Element XR (Thermo Fisher Scientific) high-resolution mass-spectrometer coupled with the Analyte Excite (Teledyne Cetac) excimer laser ablation system equipped with a HelEx II cell. The grain morphology and grain interior data were obtained from cathodoluminescence images. The parameters of mass-spectrometer measurement were optimized to obtain the maximum signal intensity of ^{208}Pb, with a minimum value of $^{248}ThO^+/^{232}Th^+$ (less than 2 %), using the NIST SRM612 standard. All measurements were made from the masses of ^{202}Hg, $^{204}(Pb+Hg)$, ^{206}Pb, ^{207}Pb, ^{208}Pb, ^{232}Th, ^{238}U. The survey was performed using E-scan mode. The signals were detected in counting mode for all isotopes except for ^{238}U and ^{232}Th (triple mode). The laser beam diameter was 35 μm, pulse repetition frequency – 5 Hz, and laser fluence – 3 J/cm^2. The mass-spectrometry data processing,

including the calculation of isotope ratios, was carried out using the GLITTER software [Griffin et al., 2008]. Considering elemental and isotope fractionation, the U-Pb isotope ratios were normalized to the corresponding isotope ratios of the Plesovice standard zircons [Slama et al., 2008]. A zircon correction for non-radiogenic lead was made based on [Andersen, 2002]. Single analytical errors (of ratios, ages) are presented at level 1σ, the errors in calculation of concordant ages and concordia intersections – at level 2σ. The concordia diagrams were plotted using Isoplot software [Ludwig, 2003].

4. STRUCTURAL PETROLOGY OF THE CONTACT ZONE

The contact of the Shivey and Chadal massifs shows a complex form of alternation of moderately to highly alkaline basic, intermediate and acidic rocks, with widespread reticulate, cuspate, palmate and patchy structures typical of mingling. The total area occupied by the displacement structures is about 12 km^2. The structural and petrologic studies made it possible to distinguish two types of mingling structures corresponding to different displacement mechanisms of magmas of contrasting compositions.

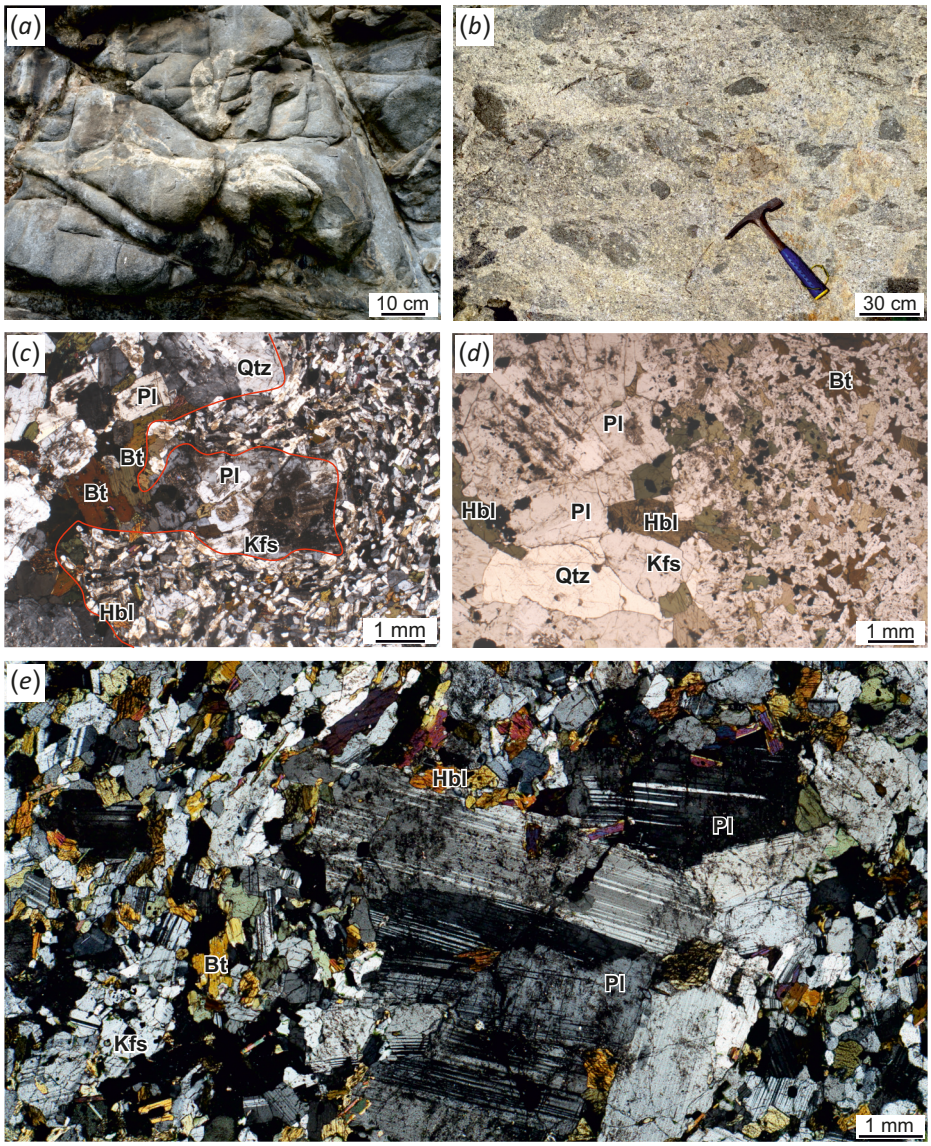

Fig. 3. The early-type mingling structures.
(*a*) – monzogabbro with granosyenite veins; (*b*) – inclusions of monzodiorites in granosyenites; (*c*) – a well-defined contact between granosyenites and monzodiorites; (*d*) – a gradational contact between granosyenites and monzodiorites; (*e*) – xenocrystic plagioclase entrapped within monzodiorite.

Рис. 3. Структуры и взаимоотношения контрастных по составу пород раннего типа минглинга.
(*a*) – монцогаббро с прожилками граносиенитов; (*b*) – включения монцодиоритов в граносиенитах; (*c*) – четкий контакт между граносиенитами и монцодиоритами; (*d*) – постепенный контакт между граносиенитами и монцодиоритами; (*e*) – захваченные вкрапленники плагиоклаза в монцодиорите.

The first-type structures represent a plutonic mingling characterized by both large (up to several meters) monzogabbro bodies with granosyenite-filled extension fractures (Fig. 3, a) and small inclusions of intermediate rocks in more acid rock varieties (Fig. 3, b). The rock contacts vary from well-defined (Fig. 3, c) to gradational, with the transition from one mineral fracture to another defined based on an increasing amount of dark-colored minerals and a gradually decreasing size of biotite and plagioclase aggregates.

The transition zones are characterized by poikilitic crystallization structures with dark-colored mineral inclusions in plagioclase (Fig. 3, d). The basic and intermediate rocks exhibit the entrapment of large granitoid-hosted plagioclase phenocrysts or intergrowth of quartz and plagioclace (Fig. 3, e).

The rocks show zones of a variable thickness in the range of about 10–15 m to 0.5 km with imposed brittle-plastic deformations and flow traces (Fig. 4). The deformations are observed both in granosyenite bodies with inclusions

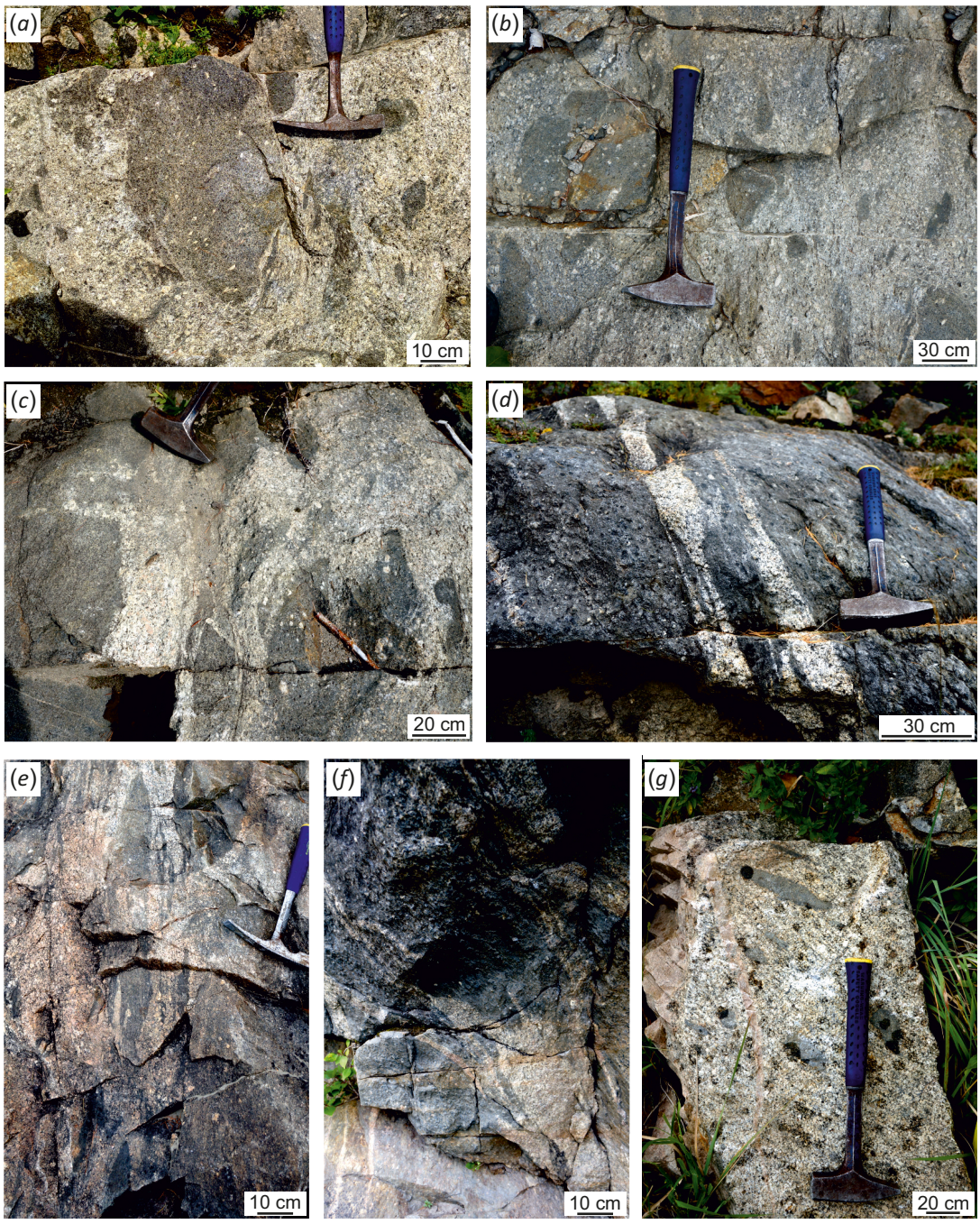

Fig. 4. Brittle-plastic deformation structures, superimposed on the early-mingling rocks.

Рис. 4. Хрупкопластичные деформационные структуры, наложенные на породы раннего минглинга.

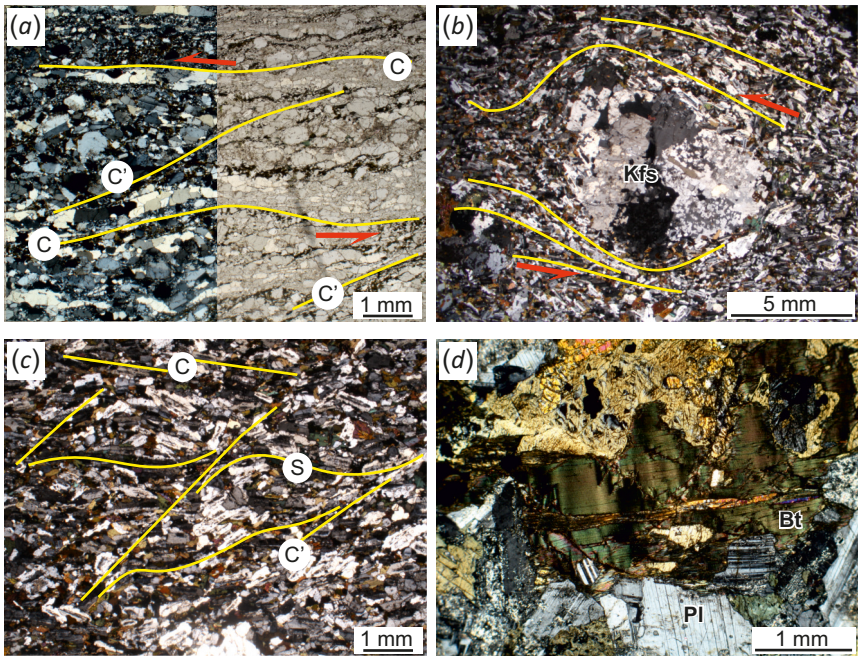

Fig. 5. Micrographs of deformation structures in rocks of the early-mingling type.
(*a*) – C/C' structures with left-lareral kinematics within blastomylonite zones in the monzodiorites; (*b*) – left-lateral rotation of a potassium feldspar phenocryst with a dislocation of the mineral internal structure; (*c*) – C/C'/S structures in monzodiorite; (*d*) – biotite kink-band structures in monzogabbro.

Рис. 5. Микрофотографии деформационных структур в породах раннего типа минглинга.
(*a*) – C/C' структуры в бластомилонитах по монцодиориту с левосторонней кинематикой; (*b*) – левостороннее вращение вкрапленника калиевого полевого шпата с нарушением внутренней структуры минерала; (*c*) – C/C'/S структуры в монцодиорите; (*d*) – структуры kink-band в биотите из монцогаббро.

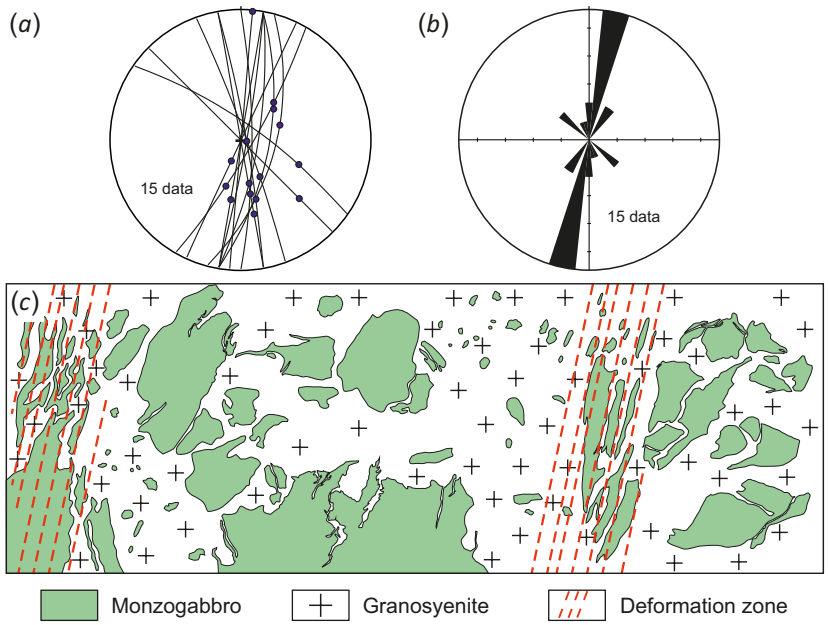

Fig. 6. Structural diagrams (*a*, *b*) and an off-scale scheme of the mingling with deformation zones (*c*).
(*a*) – arcs – shear plane orientation, points – orientation of mineral lineation (lower hemisphere, equal-angle projection); (*b*) – rose chart for shearing planes (corner sector 24°, interval 10 %). Dominant direction – 2° (7 sample measurements).

Рис. 6. Структурные диаграммы (*a*, *b*) и внемасштабная схема смешения контрастных по составу расплавов с зонами деформаций (*c*).
(*a*) – дуги – ориентировка плоскостей скалывания, точки – ориентировка минеральной линейности (нижняя полусфера, равноугольная проекция); (*b*) – роза-диаграмма для простирания плоскостей скалывания (угловой сектор 24°, интервал 10 %). Доминирующее направление – 2° (7 замеров).

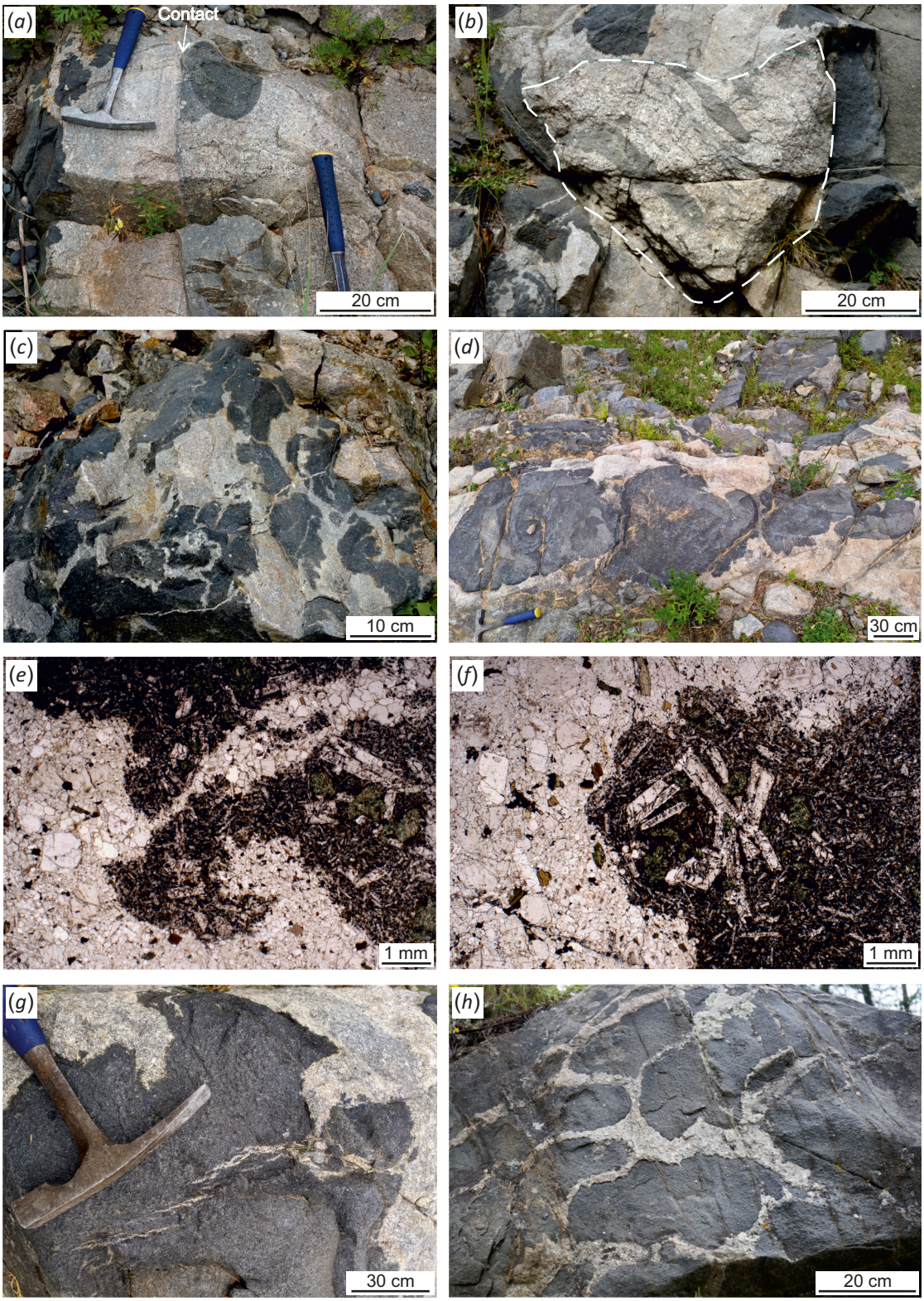

Fig. 7. The late-mingling structures.
(*a*) – crosscutting contacts with host rocks; (*b*) – xenoblocks of plutonic mingling structures in granosyenites; (*c*) – monzogabbo with granosyenite veins; (*d*) – granosyenite with monzogabbro nodules; (*e*) – bay-shaped contact between granosyenites and monzogabbro; (*f*) – granosyenite-plagioclase aggegates in monzogabbro; (*g*, *h*) – granosyenite-filled extension fractures in monzogabbro.

Рис. 7. Структуры и взаимоотношения контрастных по составу пород позднего минглинга.
(*a*) – секущие контакты с вмещающими породами; (*b*) – ксеноблоки структур плутонического минглинга в граносиенитах; (*c*) – монцогаббро с прожилками граносиенитов; (*d*) – граносиениты с нодулями монцогаббро; (*e*) – заливообразный контакт между граносиенитами и монцогаббро; (*f*) – агрегаты плагиоклаза из граносиенитов в монцогаббро; (*g*, *h*) – трещины растяжения в монцогаббро, заполненные граносиенитами.

of diorites and in mozogabbro bodies with intrusions of granite veins. The smaller basic-rock bodies occur as lenses elongated in the direction of motion (Fig. 4, c, e, g). The fractures become feather-like or flame-like, and their orientation coincides with the direction of elongation and fragmentation of diorites (Fig. 4, d, f). There were no deformations noticed in relatively large monzogabbro exposures (Fig. 4, a, b, c), though thin sections of monzogabbro exhibit numerous structures reflecting rock fragmentation and intracrystalline deformations (Fig. 5).

The observed shear deformation structures are C/C'/S structures and rotational structures of K-feldspar, plagioclase and quartz phenocrysts or intergrowths. The C/C' and C/C'/S structures with the left-lateral kinematics are observed within blastomylonite zones in the monzodiorites, quartz-and-plagioclase recrystallization, fragmentation and grain boundary sliding zones (Fig. 5, a), and in relation to the predominant orientation of plagioclase crystals (Fig. 5, c). Rotation of the K-feldspar phenocrysts gives rise to the formation of pressure shadows around the aggregates and disturbs the internal structure of a mineral (Fig. 5, b). The intracrystalline deformation structures occur also within biotite crystals in the monzogabbro with kink-band structures (Fig. 5, d). A combination of intragranular deformations, associated with wavy and mosaic extinction relative to large monocrystals, and small non-deformed aggregates implies syntectonic recrystallization in rocks.

The shear planes of granosyenites and monzodiorites are oriented submeridionally. The orientation of mineral lineation in the rocks considered and, therefore, the direction of transport of material are parallel to each other (Fig. 6, a, b). The granitoid foliation and lenticular basite zones act as planar concentrators for stress relaxation in rocks which are a result of imposed brittle-plastic tectonic deformations. The location, orientation and frequency of occurrence of these zones depend on the direction of applied forces and on rock rheology (Fig. 6, c).

These rocks (deformed or non-deformed) are intersected by the **second-type, late-mingling structures** (Fig. 7). There are well-defined contacts between the early- and late-mingling structures and xenoblocks of the deformed early-mingling rocks in the late-mingling structure (Fig. 7, a, b). The late-mingling rocks are represented by fine-grained monzogabbro and granosyenites not subjected to imposed deformations. They are characterized by cuspate contacts (Fig. 7, c, d). The rocks are clearly distinguished from each other by composition and grains and do not comprise any transition zones. The granosyenites (exposures and thin sections) exhibit the entrapped monzogabbro nodules, and the marginal parts of monzogabbro show plagioclase aggregates captured from granosyenites (Fig. 7, e, f).

The acidic and intermediate rocks have an irregular distribution in the late-mingling structures: there occur the segments composed primarily of monzogabbro with granosyenite veins and reticular-structure formation (Fig. 7, g, h) and the segments dominated by acidic rocks with entrapped single mafic inclusions. This type of mingling is dominated by basic rocks. Similar structures comprise the segments 2 to 10 m long.

5. PETROGRAPHY AND WHOLE-ROCK GEOCHEMISTRY

On the basis of the structural petrology and petrogeochemistry data, the rocks from the contact zone of the Shivey and Chadal massifs can be divided into 5 groups: salic, mafic and intermediate rocks of the early mingling; mafic and salic rocks of the late mingling. The major trace and rare-earth element contents are presented in App. 1, Table 1.1.

The early-mingling salic rocks of the early-type mingling are medium-to-coarse-grained equigranular granosyenites and granodiorites (Fig. 8, a). According to diagram SiO_2–Na_2O+K_2O (Fig. 9, a), the rocks are related to moderately alkaline and alkaline varieties.

All salic rocks of the first-type mingling are ferruginous (Fig. 9, b): #Fe=0.80–0.96. ASI values are 0.97–1.06, so that the rocks occupy an intermediate position between the metaluminous and weakly aluminous varieties (Fig. 9, d). High MALI index (7.07–10.84) in combination with low SiO_2 contents allows them to be related to the alkaline type (Fig. 9, c). The salic rocks of the early mingling exhibit a decrease in $Fe_2O_3^T$, Al_2O_3, MgO, Eu and Zr contents with an increase in their silica acidity (Fig. 10).

The REE distribution spectra (Fig. 11, a) demonstrate a relatively high REE concentration, light REE enrichment ($(La/Yb)_n$–9.11–13.65), an insignificant differentiation of heavy REE ($(Gd/Yb)_n$–1.53–2.01), a negative europium anomaly (Eu/Eu*–0.59–0.60), and its absence (Eu/Eu*–1.10) (App. 1, Table 1.1). The spider diagrams (Fig. 11, a) show Ti and Sr depletion. The differences observed in this group emphasize the irregular distribution of plagioclase in the rocks.

The mafic rocks of the early-mingling type are represented primarily by small-to-medium-grained amphibole monzogabbro and monzodiorites, the accessory minerals exhibit a wide occurrence of sphene (see Fig. 8, b). The dark-colored ones often form a glomeroporphyric structure. Total alkalinity implies that the rocks are alkaline and moderately alkaline (see Fig. 9, a).

The rocks show a decrease in $Fe_2O_3^T$, CaO and MgO contents with increasing silica content; Al_2O_3 and K_2O contents and silica content are uncorrelated (see Fig. 10).

The rare-earth element distribution spectra show LREE ($(La/Yb)_n$–8.47–11.46) enrichment, HREE ($(Gd/Yb)_n$–2.16–2.89) differentiation, and poorly defined or no europium anomaly (Eu/Eu*–0.88–1.01) in the rocks (Fig. 11, c; App. 1, Table 1.1). The spider-diagrams demonstrate the rock

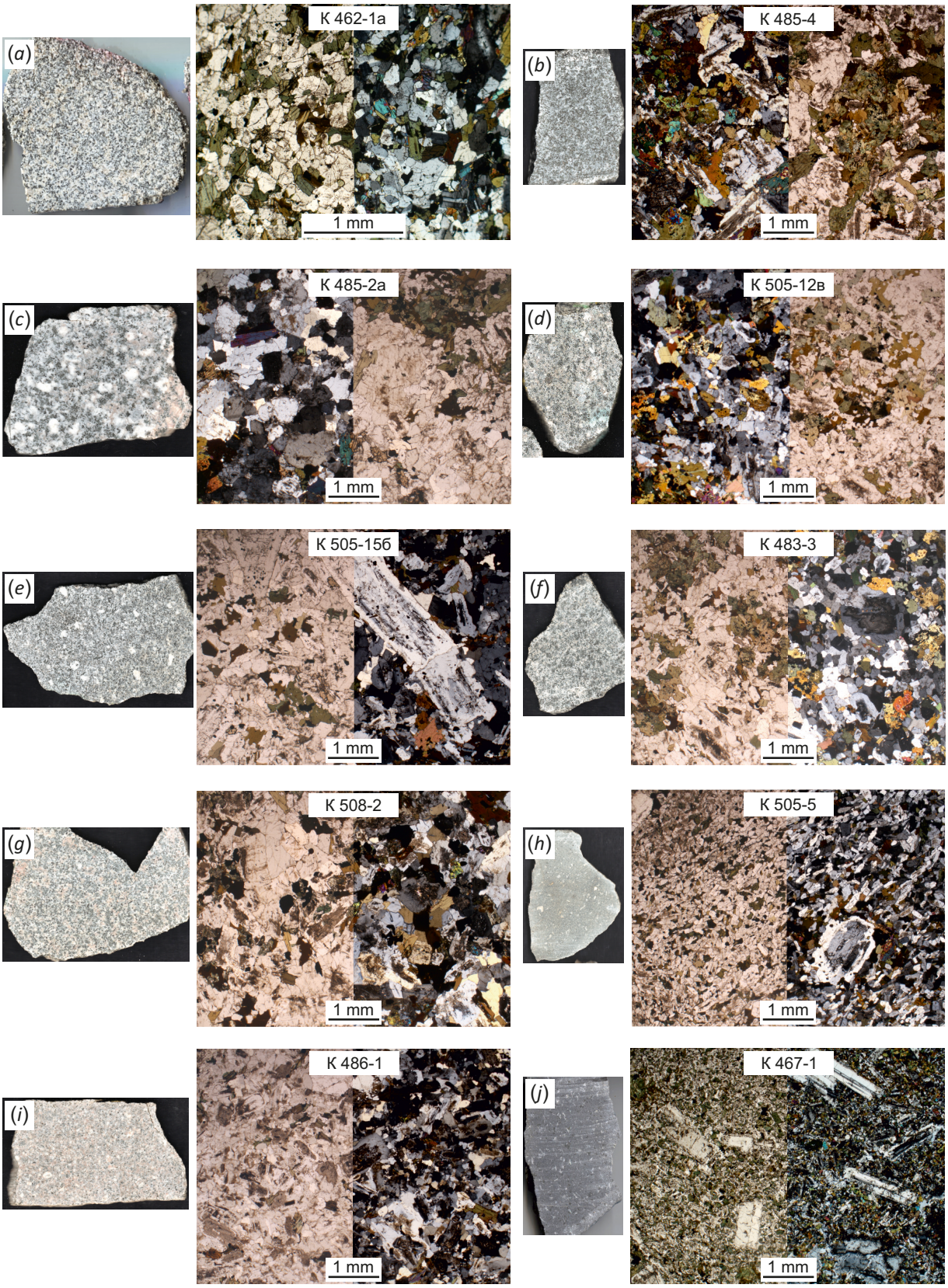

Fig. 8. Petrography of the Shivey and Chadal massifs.
(*a*) – granosyenite of the early mingling; (*b*) – monzogabbro of the early mingling; (*c*–*h*) – intermediate rocks; (*i*) – granosyenite of the late mingling; (*j*) – monzodiorite of the late mingling.

Рис. 8. Петрография пород Шивейского и Чадалского массивов.
(*a*) – граносиенит раннего минглинга; (*b*) – монцогаббро раннего минглинга; (*c*–*h*) – породы переходного состава; (*i*) – граносиенит позднего минглинга; (*j*) – монцодиорит позднего минглинга.

enrichment in lithophylic and high field strength elements with large ions, insignificant Ta-Nb anomaly and poorly defined Ti minimum (Fig. 11, d).

The early-mingling intermediate rocks are assigned the samples showing compositional variation from monzonites to quartz syenites. The rocks vary from coarse-to-moderate-grained, equigranular to fine-grained porphyric with plagioclase and K-feldspar phenocrysts (see Fig. 8, c–h).They are also characterized by poikilitic structures, with chadacrysts represented by dark-colored minerals (pyroxene and amphibole) and oikocrysts represented by plagioclase and K-feldspar. Plagioclase crystals (both in inclusions and groundmass) in all intermediate rocks have a zonal structure with inclusions in the central part. Of the accessory minerals, apatite and sphene are of widespread occurrence. The latter forms large wedge-shaped aggregates and frequently occurs in the form of poikilitic intergrowths in K-feldspar.

Total alkalinity implies that the rocks are moderately alkaline (see Fig. 9). The fields of contents of petrogenic oxides in hybrid rocks in binary diagrams lie in an intermediate area between mafic and salic rocks tending to monzogabbro and monzodiorites and creating a single distribution trend (see Fig. 10). However, the behavior of rare-earth elements (Eu, Sr) in binary diagrams (see Fig. 10) coincides with trends in distribution of these elements in

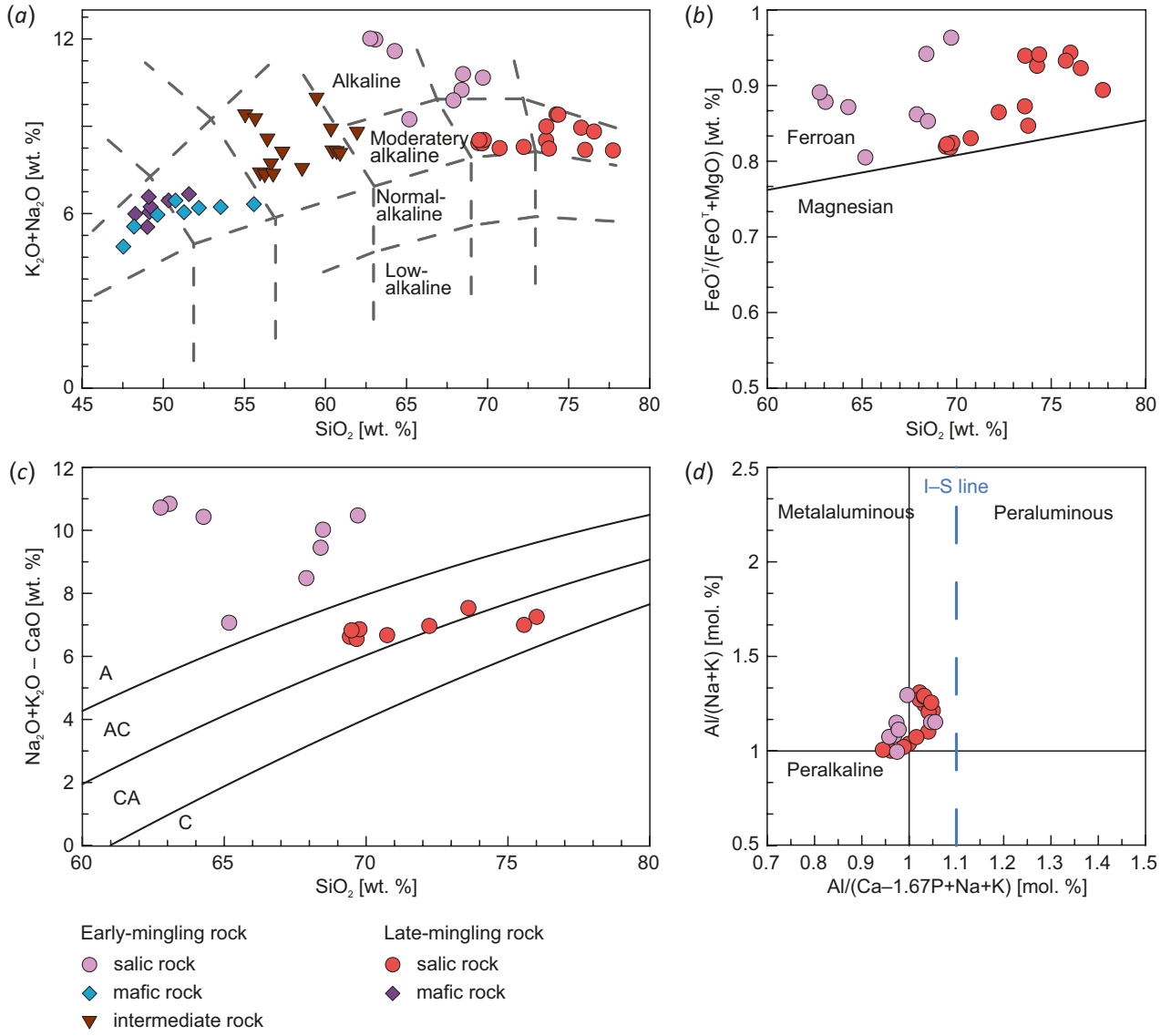

Fig. 9. Classification diagrams for early- and late-mingling types.
(*a*) – K_2O+Na_2O – SiO_2 (classification boundaries after [Petrographic Code..., 2009]); (*b*) – FeO*/(FeO*+MgO) – SiO_2 [Frost et al., 2001]; (*c*) – MALI – SiO_2 [Frost et al., 2001]; (*d*) – A/CPNK, I-S line after [Chappell, White, 2001].

Рис. 9. Классификация пород раннего и позднего минглинга.
(*a*) – диаграмма K_2O+Na_2O – SiO_2 (классификационные границы по [Petrographic Code..., 2009]); (*b*) – диаграммы FeO*/(FeO*+MgO) – SiO_2 по [Frost et al., 2001]; (*c*) – MALI – SiO_2 по [Frost et al., 2001]; (*d*) – диаграмма A/CPNK, I-S линия по [Chappell, White, 2001].

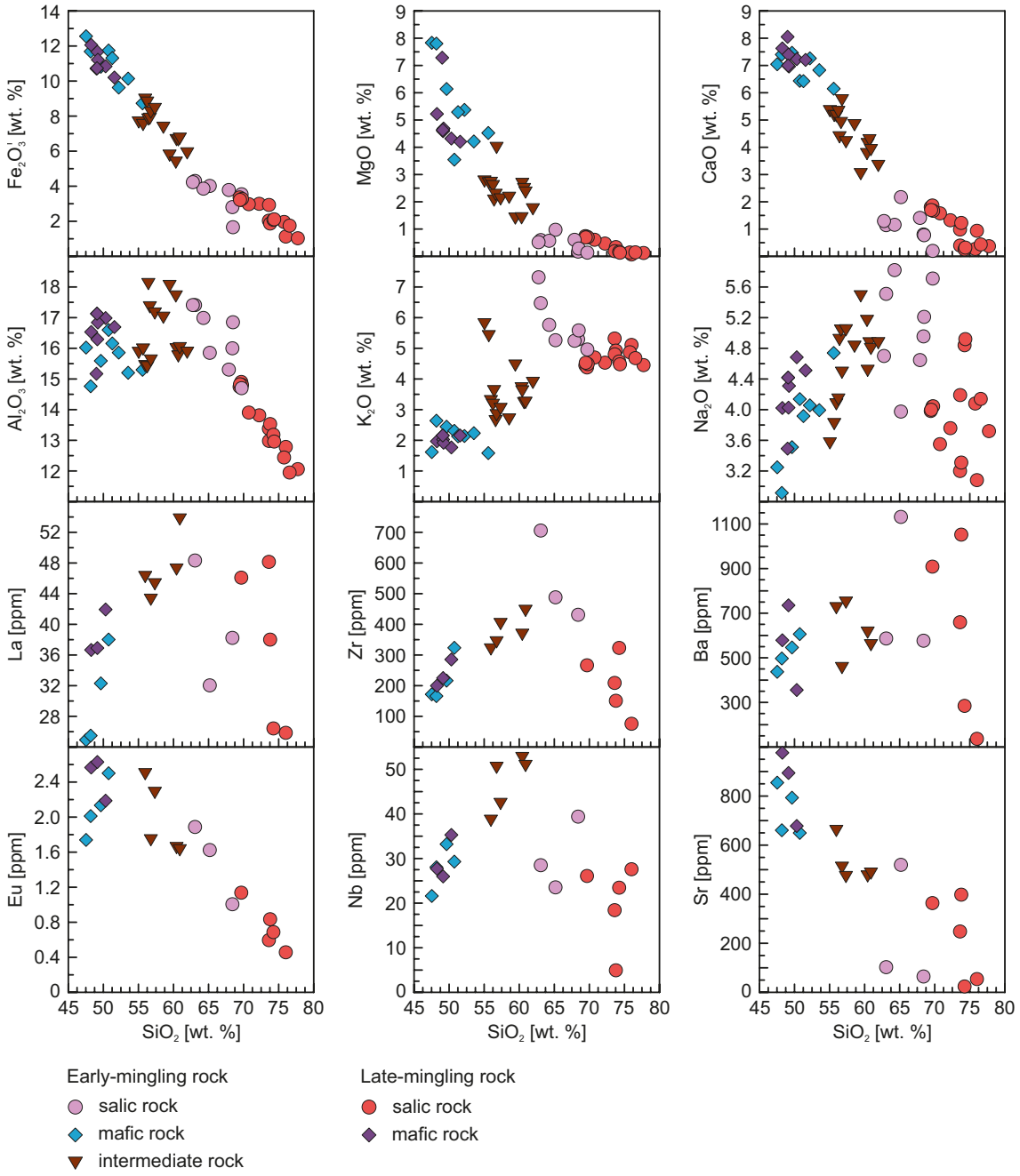

Fig. 10. Binary diagrams for rocks of the early- and late-mingling types.

Рис. 10. Бинарные диаграммы для пород раннего и позднего минглинга.

acid rocks. The fields of Ba, La and Zr contents constitute intermediate areas between mafic and salic melts and create distribution trends of their own (see Fig. 10).

REE distribution spectra (Fig. 11, e) demonstrate enrichment in light REE ($(La/Yb)_n$–8.32–11.97) and insignificant differentiation in heavy REE ($(Gd/Yb)_n$–1.66–2.50) (App. 1, Table 1.1). The intermediate rocks are characterized by ill- and well-defined negative europium anomalies (Eu/Eu*–0.57–0.87). The spider-diagrams show rock enrichment in LILE, ill-defined Ta-Nb anomaly, and negligible Sr and Ti minimums (Fig. 11, f).

The late-mingling salic rocks are represented by fine-grained granosyenites characterized by up to 1-cm porphyry-contained phenocrysts of K-feldspar and plagioclase. The phenocrysts are zonal, with small dark-colored intergrowths often exhibited in the central part. The groundmass is fine-grained, with isometric quartz, plagioclase and K-feldspar aggregates (see Fig. 8, i). In SiO_2–Na_2O+K_2O diagram, these rocks occupy the field of moderately alkaline varieties (see Fig. 9, a).

The second-type-mingling granosyenites are ferriferous, low-aluminous, alkali-calcic and calc-alkali: #Fe=0.82–0.94;

ASI=0.94–1.05; MALI=6.55–9.16 (see Fig. 9, b, c, d), characterized by trends of decrease in $Fe_2O_3^T$, CaO, Al_2O_3 and MgO contents and increase in K_2O content with increasing silica content of rock (see Fig. 10). With increasing SiO_2. content, there is Eu, Sr and Zr depletion (see Fig. 10).

REE distribution spectra (Fig. 11, a) reveal significant LREE enrichment ($(La/Yb)_n$–6.47–26.31), HREE differentiation, and negative europium anomalies (Eu/Eu*–0.39–0.85) (App. 1, Table 1.1). The multi-element diagrams show Ti and Sr minimums, and there can be observed Ta-Nb anomaly in two samples (Fig. 11, b).

The late-mingling maphic rocks include fine-grained hornblende monzogabbro characterized by porphyric (long-prismatic plagioclase aggregates) and evenly-grained structure (see Fig. 8, j). Total alkalinity implies that the rocks are alkaline (see Fig. 9, a). The rocks exhibit trends for decrease in $Fe_2O_3^T$, CaO and MgO contents with increasing silica and Zr and Nb contents (see Fig. 10).

The late-mingling mafic rocks show LREE enrichment ($(La/Yb)_n$–13.15–14.75), HREE differentiation ($(Gd/Yb)_n$–2.60–3.28), and ill-defined europium anomalies (Eu/Eu*–0.88–0.97) (Fig. 11, c; App. 1, Table 1.1). The spider-diagrams display the enrichment of large-ion lithophile elements in rocks and negligible Ta-Nb and Ti anomalies (Fig. 11, d).

6. ZIRCON U-PB GEOCHRONOLOGY

The age determination for both-type mingling rocks involved the studies of zircons from early-mingling basites and late-mingling granitoids.

Sample K 467-2 (51°20'04.67" N, 96°22'22.98" E) was taken from fine-grained granosyenites, intersecting the plutonic mingling structures with features of hybridization. The zircon monofraction is represented by half-transparent and transparent idiomorphic prismatic yellow-pale crystals with well-defined edges and smooth faces. The grains vary in size from 100 to 300 μm in long dimension

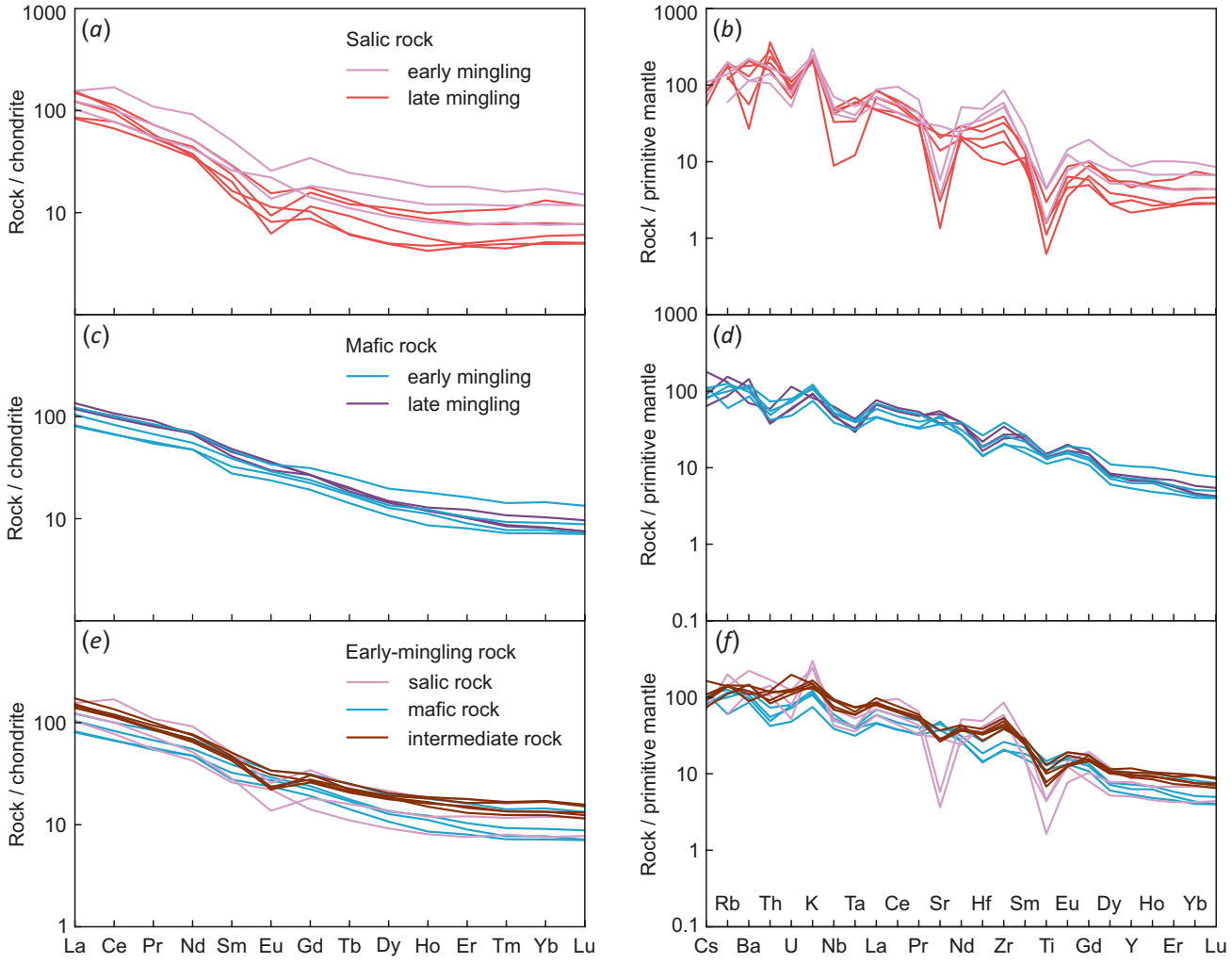

Fig. 11. The REE distribution spectra (*a*, *b*, *c*) – CI chondrite-normalized [Boynton, 1984]; (*d*, *e*, *f*) – primitive mantle-normalized [Taylor, McLennan, 1985].

Рис. 11. Спектры распределения РЗЭ (*a*, *b*, *c*) (нормированы по хондриту CI [Boynton, 1984]) и спайдер-диаграммы (*d*, *e*, *f*) (нормированы по примитивной мантии [Taylor, McLennan, 1985]).

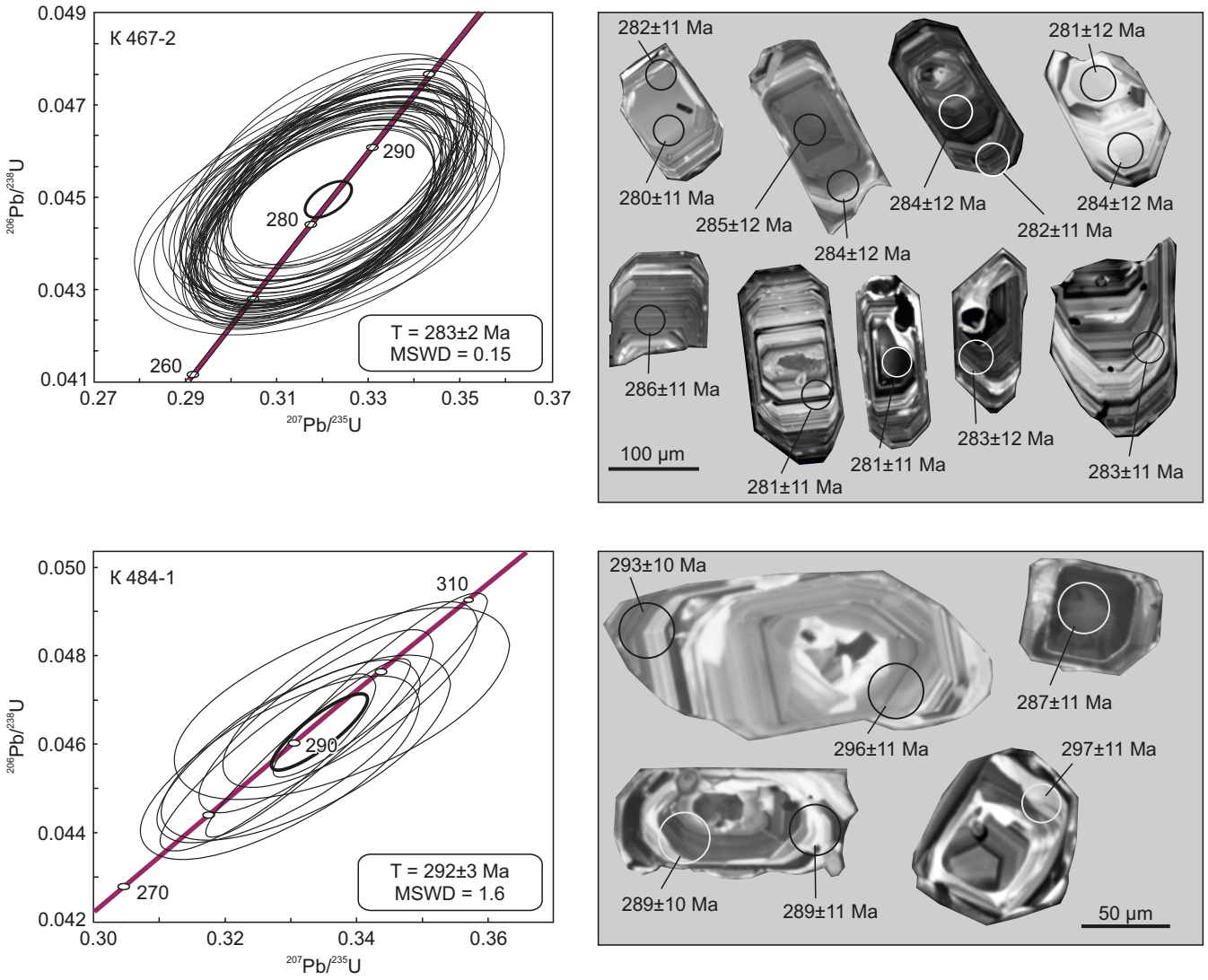

Fig. 12. Concordia diagrams and CL-images of zircons from the Shivey and Chadal massifs, showing the analyzed sampling points and relevant ages (Pb^{206}/U^{238}).

Рис. 12. Диаграммы с конкордиями и катодолюминесцентное изображение цирконов из пород Шивейского и Чадалского массивов с точками измерений и возрастом (Pb^{206}/U^{238}).

and from 40 to 60 μm in width. The cathodoluminescence (CL) of zircons showed a thin oscillatory magmatic zoning (Fig. 12). The analysis (App. 1, Table 1.2; Fig. 12) made on 50 local points of magmatic zircon yields a concordant age of 283±2 Ma (MSDW=0.15).

Sample К 484-1 (51°20'04.07" N, 96°22'20.08" E) was taken from the early-mingling small-grained monzodiorites. The zircon monofraction is represented by half-transparent idiomorphic prismatic yellow-pale crystals with well-defined edges and smooth faces. The grains vary in size from 50 to 150 μm in long dimension and from 50 to 70 μm in width. The cathodoluminescence (CL) of zircons showed a thin oscillatory magmatic zoning (Fig. 12). Isotope ratios obtained for 9 local points of magmatic zircon (App. 1, Table 1.2; Fig. 12) show a concordant age of 292±3 Ma (MSDW=1.6).

7. DISCUSSION OF RESULTS

The study of the Late Paleozoic magmatism in the eastern Kaakhem area revealed two divergent stages in formation of rock associations of contrasting composition at 290–280 Ma. Both stages are characterized by simultaneous mafic and salic melt intrusion and mingling-structure formation.

Mafic and salic source rocks. The petrographic and petrogeochemical data on mafic rocks show that the early- and late-mingling basites originated from a single magmatic source. Enrichment of alkalis, Ti, REE, LILE and HFSE in the rocks and ill-defined Ta-Nb anomalies allow the basite source to be assigned to an enriched intraplate type (Fig. 13, a, b). Successive intrusion of basite melts from a single source indicates high permeability in the lithosphere at 290–280 Ma.

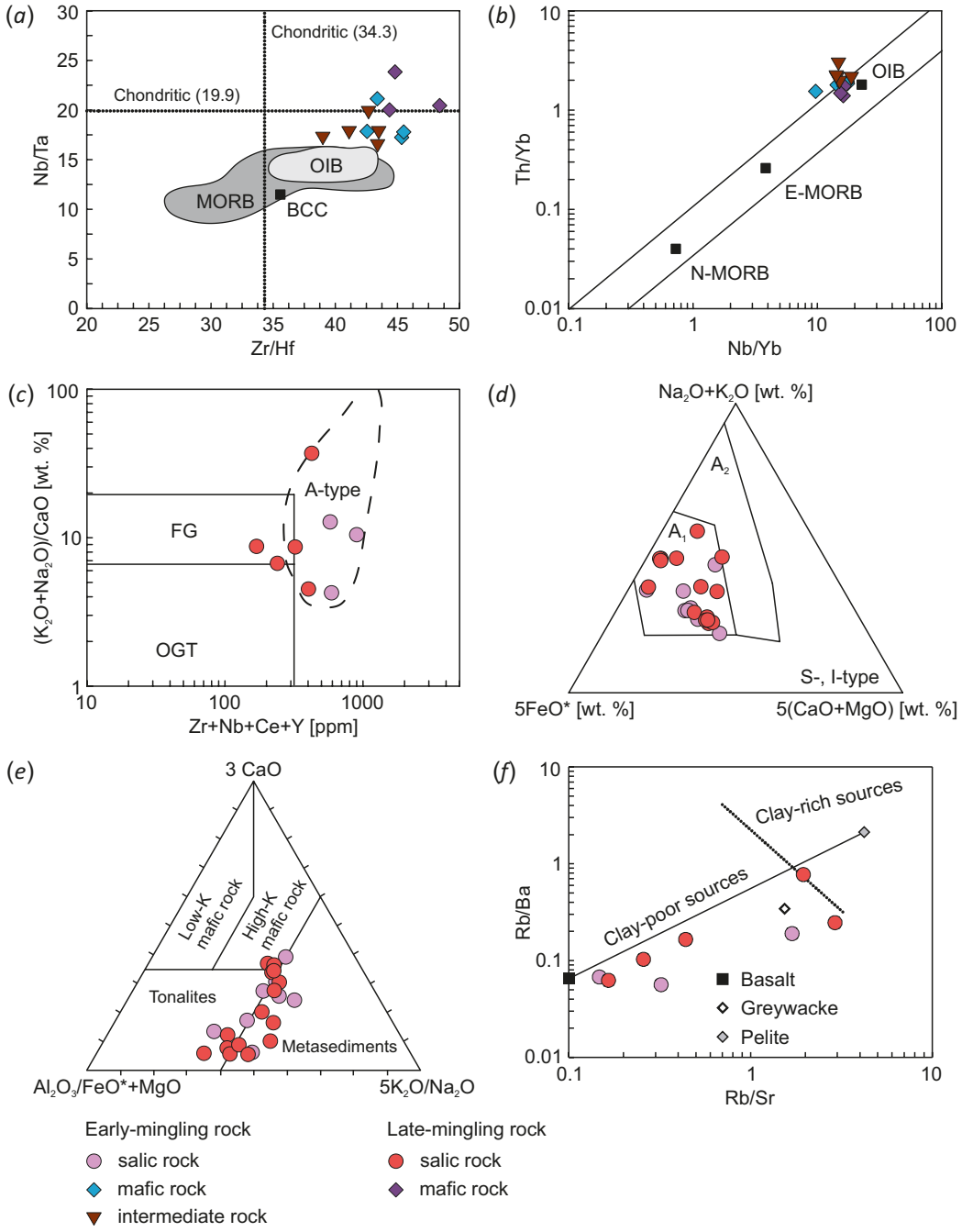

Fig. 13. Classification diagrams for mafic (*a*, *b*) and salic (*c*, *d*) rocks.
(*a*) – Nb/Ta – Zr/Hf [Munker et al., 2003]; (*b*) – Th/Yb – Nb/Yb [Pearce, 2008]; (*c*) – $(K_2O+Na_2O)/CaO$ – Zr+Nb+Ce+Y [Whalen et al., 1987]; (*d*) – Na_2O+K_2O – 5FeO* – 5(CaO+MgO) [Grebennikov, 2014]; (*e*) – 3CaO – Al_2O_3/FeO*+MgO – $5K_2O/Na_2O$ [Laurent et al., 2014]; (*f*) – Rb/Ba – Rb/Sr [Sylvester, 1998].
(*a*–*b*) – MORB – mid-ocean ridge basalts, E-MORB – enriched mid-ocean ridge basalts, N-MORB – normal mid-ocean ridge basalts, OIB – oceanic-island basalts, BCC – bulk continental crust. (*c*–*d*) – FG – fractionated granite; OGT – unfractionated M-, I- and S-type granites; A_1 – granites formed as a result of differentiation of alkaline-basaltic magmas, with insignificant assimilation processes; A_2 – granites, the characteristics of which are due to significant impact of contamination of mantle melts with acidic material of the continental crust.

Рис. 13. Классификационные диаграммы для мафических (*a*, *b*) и салических пород (*c*, *d*).
(*a*) – Nb/Ta – Zr/Hf [Munker et al., 2003]; (*b*) – Th/Yb – Nb/Yb [Pearce, 2008]; (*c*) – $(K_2O+Na_2O)/CaO$ – Zr+Nb+Ce+Y [Whalen et al., 1987]; (*d*) – Na_2O+K_2O – 5FeO* – 5(CaO+MgO) [Grebennikov, 2014]; (*e*) – 3CaO – Al_2O_3/FeO*+MgO – $5K_2O/Na_2O$ [Laurent et al., 2014]; (*f*) – Rb/Ba – Rb/Sr [Sylvester, 1998].
(*a*–*b*) – MORB – базальты СОХ, E-MORB – обогащенные базальты СОХ, N-MORB – нормальные базальты СОХ, OIB – базальты океанических островов, BCC – валовая континентальная кора. (*c*–*d*) – FG – фракционированные граниты; OGT – нефракционированые граниты M-, I- и S-типа; A_1 – граниты, возникшие в результате дифференциации щелочно-базальтовых магм при незначительных процессах ассимиляции; A_2 – граниты, характеристики которых обусловлены значительным контаминирующим воздействием мантийных расплавов с кислым материалом континентальной коры.

The intermediate rocks were only formed at the first stage of mixing of magmas of contrasting composition. The trends in the distribution of petrogenic oxides and rare-earth elements (see Fig. 10) correspond to those in mafic rocks, and the negative europium anomalies (Eu/Eu*= =0.57–0.87) indicate plagioclase fractionation typical of salic rocks. The lack of detailed mineralogical studies does not enable identifying the genesis of intermediate rocks unambiguously; however, already at this stage there is an opportunity to relate their formation at least to solid transportation back and forth at the coexistence of contrasting magmas [Hibbard, 1991; Ubide et al., 2014].

The early- and late-mingling salic rocks are assigned to A_1-type granitoids in accordance with their petrogeochemical characteristics [Whalen et al., 1987] и [Grebennikov, 2014] (Fig. 13, c, d). A well-defined Ta-Nb anomaly and Sr and Ti minimums (see Fig. 11, b) in granites and granosyenites are indicative of the crustal substrate. The diagram showing the experimental data on melting of diverse source regions [Laurent et al., 2014] exhibits granosyenites and granites located between the tonalite fields and metasedimentary rocks (Fig. 13, e). A small part of the samples falls within the field of high-K mafic rocks. Rb/Sr and Rb/Ba values are ranging from 0.15–1.69 to 0.06–0.19 for granosyenites and from 0.17–2.91 to 0.06–0.77 for granites (Fig. 13, f), which indicates the mixed protolith contributed to by both metapelites and basites. This has been confirmed by isotope research results: εNd(T) values for alkaline syenites from the Shivey massif are +3.4 [Sugorakova, 2017].

The most likely protolith of granitoids from the Shivey massif are tonalities and metasedimentary rocks of the continental crust formed during the stage of regional subduction or collision. In the Early Permian, the lower-crustal substrate melting occurred due to supply of heat at the juvenile melting whose differentiates are the rocks from the Chadal massif.

Salic rock melting was associated with plagioclase fractionation which is indicated by a decrease in CaO, Al_2O_3, Sr and Eu contents with increasing silica content (see Fig. 10). Petrogeochemical trends are seen as the result of a systematic evolution of melting from the early-mingling granosyenites to the late-mingling granites.

A wide petrographic variety and structural position of the early-mingling salic rocks allow characterizing their crystallization conditions as highly unstable. The formation and the consolidation of the melting occurred under conditions of the crust-mantle interaction and active short-term tectonic deformations.

The late-mingling salic rocks are more persistent in composition and represent the product of residual acidic melt crystallization. These rocks do not show evidence of chemical interaction between salic and mafic melts. This is also indicated indirectly by low K_2O content in granites.

Formation of mingling structures and a role of tectonic deformations. The present understanding of mixing of magmas of contrasting composition to form plutonic-mingling structures typical of the early-stage mingling is that it may occur through the injection of basite magma into the basal and middle parts of unconsolidated granitoid magma chamber [Barbarin, 2005]. A necessary condition for vertical movement of denser basite magma in the granitoid chamber is the emergence of basal inhomogeneity in the granite chamber due to short-term tectonic activity [Polyansky et al., 2017]. Imposed deformations recorded in the early-mingling rocks unambiguously imply occurrence of pulse-like tectonic deformations therein. Therefore, the implication would be that there also occurred an earlier short-term event which gave rise to the formation of the area of local disturbance and to further movement and displacement of melts due to viscosity contrasts and density differences in absence of tectonic deformations.

The movement of basic and intermediate magmas towards the upper granitoid chamber lasted until the degree of crystallinity of granitoids reached the second rheological threshold above which the magma flow acquires a rigid fabric and is no longer continuous [Rosenberg, Handy, 2005]. The subsequent release of accumulated stress gave rise to the formation of linear zones of distribution of deformation structures imposed on the rocks that had already been partially recrystallized. The deformation kinematics (left-lateral strike-slip) corresponds to the extensional environment.

The late-mingling structures embody the characteristics of contrasting rock associations formed through the injection of basite magma into acid magma [Litvinovsky et al., 1995; Ubide et al., 2014]. The injection of the second-phase granosyenite magma along the early-mingling rock zones of weakness took place under short-term shearing conditions when the duration of the deformation process is much lower than the rate of consolidation of the rocks. The subsequent intrusion of magma into unconsolidated granocyenites of the monzodiorite magma caused the formation of contact cuspate mingling-structures. The temperature contrast in displacement accelerates the consolidation of more basic magma which is accompanied by the occurrence of contractional fractures filled with salic material later on.

Geodynamic implications. A structural and petrologic study of the Early Permian basite and acid magmatism occurrences showed their inseparable connection with the extensional processes. The data obtained for the composition of basalts from the Chadal massif imply an enriched intraplate magma source. A combination of mantle heat and tectonic extension environments gave rise to the occurrence of pulse-like periods of the Early Permian gabbro-syenite magmatism in the eastern Kaakhem area which is typical

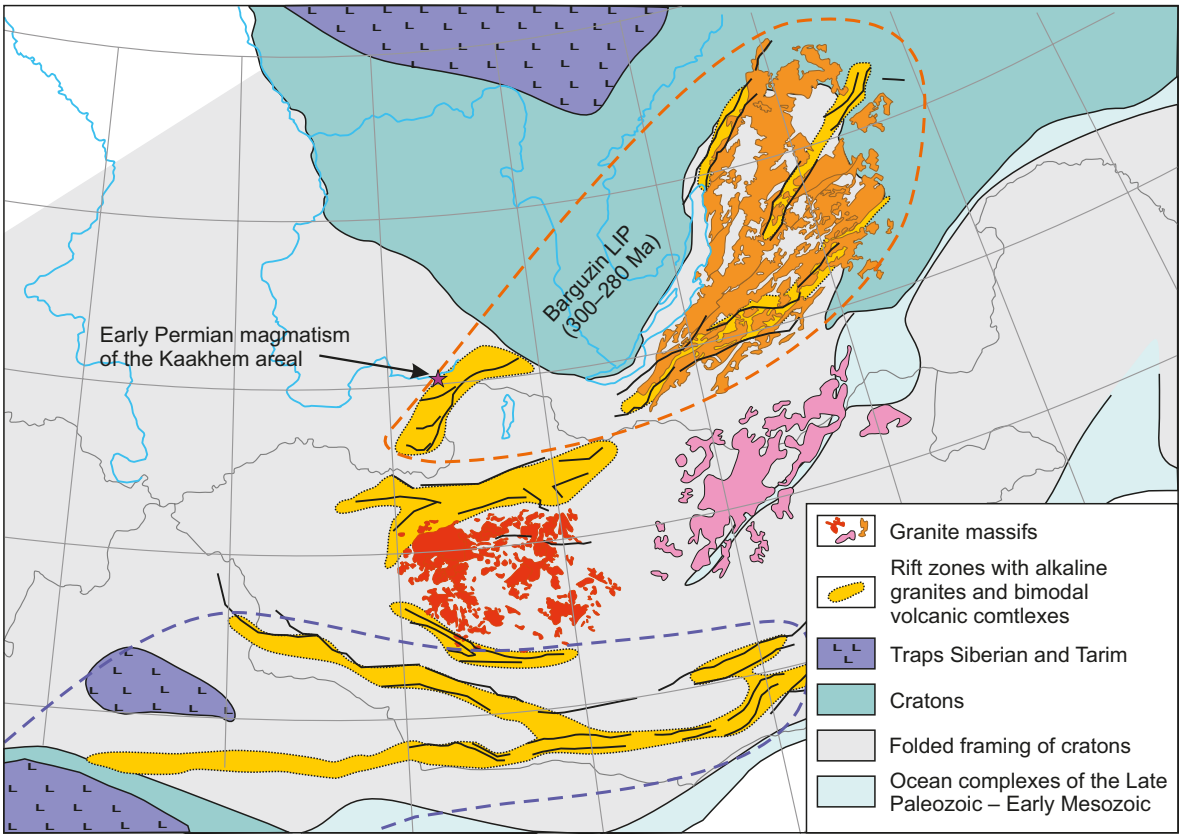

Fig. 14. Location of the Barguzin large igneous province (LIP) in the Central Asian orogenic belt (after [Yarmolyuk et al., 2013, 2019]).

Рис. 14. Расположение Баргузинской крупной изверженной провинции (LIP) в структурах Центрально-Азиатского складчатого пояса (по [Yarmolyuk et al., 2013, 2019], с упрощениями и дополнением).

of the Late Paleozoic CAOB evolution [Kozlovsky et al., 2012; Khromykh et al., 2018; Yarmolyuk et al., 2019].

The period of occurrence of high-alkali gabbro-granite magmatism in the Kaakhem area (290–280 Ma) suggests it to be a part of the Late Paleozoic development of the East Sayan alkali-granitoid province. According to [Yarmolyuk et al., 2013, 2019], these magmatic formations are a part of the Baguzin large igneous province (LIP) (Fig. 14). It is comprised by several rift zones associated with high-alkali bimodal magmatism occurrences in the period of 300 to 280 Ma. In particular, the Eastern Sayan rift zone along the eastern boundary between Tuva and Eastern Sayan Mountains exhibits gabbro-syenite associations [Yarmolyuk et al., 2013]. Since the formation of most of the granitoids in the Kaakhem area (512–445 Ma) occurred at the accretion-collision stage [Rudnev et al., 2015; Sugorakova, Khertek, 2017], the formation of the Chadal and Shivey massif may be assigned to the post-collisional (intraplate) stage in the evolution of the region.

8. CONCLUSION

In the eastern Kaakhem batholith, there occurred two stages of contrasting magmatism in the period 292–283 Ma. The early stage is characterized by formation of the plutonic mingling structures and intermediate rocks. The late stage represents a subsequent injection of acid and basic magmas into the local extension zones with the mingling-structure formation.

There were first obtained the specific data on tectonic regimes and deformation kinematics in the Early Permian intacontinental rift environments. The stress release was short-term and periodical, and the deformation structures are brittle-plastic and formed synchronously with the contrasting magmatic associations.

Petrogeochemical composition of the early- and late-mingling basites implies a single enriched magma source. The formation of gratosyenites and granites is related to melting of tonalites and metasediments with a significant contribution of the mantle component.

The formation of the Chadal and Shivey granitoid massifs occurred at the intraplate stage of development of the Early Permian Eastern Tuva geological structures.

9. ACKNOWLEDGEMENTS

The authors would like to express their sincere gratitude to V.V. Yarmolyuk, Academician RAS, S.V. Khromykh, Dr. Sci. (Geol.-Min.), and M.L. Kuibida, Cand. Sci. (Geol.-Min.) for an active discussion of the work.

10. CONTRIBUTION OF THE AUTHORS / ЗАЯВЛЕННЫЙ ВКЛАД АВТОРОВ

The authors contributed equally to this article.

Все авторы внесли эквивалентный вклад в подготовку публикации.

11. CONFLICT OF INTERESTS / КОНФЛИКТ ИНТЕРЕСОВ

The authors have no conflicts of interest to declare. All authors have read and agreed to the published version of the manuscript.

Авторы заявляют об отсутствии у них конфликта интересов. Все авторы прочитали рукопись и согласны с опубликованной версией.

12. REFERENCES

Andersen T., 2002. Correction of Common Lead in U-Pb Analyses That Do Not Report ^{204}Pb. Chemical Geology 192 (1–2), 59–79. https://doi.org/10.1016/S0009-2541(02)00195-X.

Barbarin B., 2005. Mafic Magmatic Enclaves and Mafic Rocks Associated with Some Granitoids of the Central Sierra Nevada Batholith, California: Nature, Origin, and Relations with the Hosts. Lithos 80 (1–4), 155–177. https://doi.org/10.1016/j.lithos.2004.05.010.

Boynton W.V., 1984. Cosmochemistry of the Rare Earth Elements: Meteorite Studies. Rare Earth Element Geochemistry. Developments in Geochemistry 2, 63–114. https://doi.org/10.1016/B978-0-444-42148-7.50008-3.

Chappell B.W., White A.J.R., 2001. Two Contrasting Granite Types. 25 Years Later. Australian Journal of Earth Sciences 48 (4), 489–499. https://doi.org/10.1046/j.1440-0952.2001.00882.x.

Dobretsov N.L., Borisenko A.S., Izokh A.E., Zhmodik S.M., 2010. A Thermochemical Model of Eurasian Permo-Triassic Mantle Plumes as a Basis for Prediction and Exploration for Cu-Ni-Pge and Rare-Metal Ore Deposits. Russian Geology and Geophysics 51 (9), 903–924. https://doi.org/10.1016/j.rgg.2010.08.002.

Frost B.R., Barnes C.G., Collins W.J., Arculus R.J., Ellis D.J., Frost C.D., 2001. A Geochemical Classification for Granitic Rocks. Journal of Petrology 42 (11), 2035–2048. https://doi.org/10.1093/petrology/42.11.2033.

Grebennikov A.V., 2014. A-Type Granites and Related Rocks: Petrogenesis and Classification. Russian Geology and Geophysics 55 (9), 1356–1373. https://doi.org/10.1016/j.rgg.2014.08.003.

Griffin W.L., Powell W.J., Pearson N.J., O'Reilly S.Y., 2008. GLITTER: Data Reduction Software for Laser Ablation ICPMS. In: P.J. Sylvester (Ed.), Laser Ablation-ICP-MS in the Earth Sciences: Current Practices and Outstanding Issues. Mineralogical Association of Canada Short Course Series. Vol. 40. Vancouver, p. 308–311.

Hibbard M.J., 1991. Textural Anatomy of Twelve Magma-Mixed Granitoid Systems. In: J. Didier, B. Barbarin (Eds), Enclaves and Granite Petrology. Developments in Petrology 13, 431–444.

Khromykh S.V., Tsygankov A.A., Burmakina G.N., Kotler P.D., Sokolova E.N., 2018. Mantle-Crust Interaction in Petrogenesis of the Gabbro-Granite Association in the Preobrazhenka Intrusion, Eastern Kazakhstan. Petrology 26, 368–388. https://doi.org/10.1134/S0869591118040045.

Kozlovsky A.M., Yarmolyuk V.V., Salnikova E.B., Travin A.V., Kotov A.B., Plotkina J.V., Kudryashova E.A., Savatenkov V.M., 2015. Late Paleozoic Anorogenic Magmatism of the Gobi Altai (SW Mongolia): Tectonic Position, Geochronology and Correlation with Igneous Activity of the Central Asian Orogenic Belt. Journal of Asian Earth Science 113 (1), 524–541. https://doi.org/10.1016/j.jseaes.2015.01.013.

Kozlovsky A.M., Yarmolyuk V.V., Travin A.V., Salnikova E.B., Anisimova I.V., Plotkina Yu.V., Savatenkov V.M., Fedoseenko A.M., Yakovleva S.Z., 2012. Stages and Regularities in the Development of Late Paleozoic Anorogenic Volcanism in the Southern Mongolia Hercynides. Doklady Earth Science 445, 811–817. https://doi.org/10.1134/S1028334X12070239.

Kuzmichev A.B., 2004. Tectonic History of the Tuva-Mongolian Massif: Early Baikal, Late Baikal and Early Caledonian Stages. Probel-2000, Moscow, 192 p. (in Russian) [Кузьмичев А.Б. Тектоническая история Тувино-Монгольского массива: раннебайкальский, позднебайкальский и раннекаледонский этапы. М.: Пробел-2000, 2004. 192 с.].

Kuz'min M.I., Yarmolyuk V.V., Kravchinsky V.A., 2011. Phanerozoic Within-Plate Magmatism of North Asia: Absolute Paleogeographic Reconstructions of the African Large Low-Shear-Velocity Province. Geotectonics 45, 415–438. https://doi.org/10.1134/S0016852111060045.

Laurent O., Martin H., Moyen J.F., Doucelance R., 2014. The Diversity and Evolution of Late-Archean Granitoids: Evidence for the Onset of "Modern-Style" Plate Tectonics between 3.0 and 2.5 Ga. Lithos 205, 208–235. https://doi.org/10.1016/j.lithos.2014.06.012.

Litvinovsky B.A., Zanvilevich A.N., Kalmanovich M.A., 1995. Multiple Displacements of Coexisting Syenite and Basite Magmas and Their Petrological Importance, Ust-Khilok Massif, Transbaikalia. Petrology 3 (2), 133–157 (in Russian) [Литвиновский Б.А., Занвилевич А.Н., Калманович М.А. Многократное смешение сосуществующих сиенитовых и базитовых магм и его петрологическое значение, Усть-Хилокский массив, Забайкалье // Петрология. 1995. Т. 3. № 2. С. 133–157].

Ludwig K.R., 2003. ISOPLOT/Ex: A Geochronological Toolkit for Microsoft Excel. Version 3.00. Berkeley Geochronology Center Special Publication 4, 74 p.

Munker C., Pfander J.A., Weyer S., Buchl A., Kleine T., Mezger K., 2003. Evolution of Planetary Cores and the

Earth–Moon System from Nb/Ta Systematic. Science 301 (5629), 84–87. https://doi.org/10.1126/science.1084662.

Pearce J.A., 2008. Geochemical Fingerprinting of Oceanic Basalts with Applications to Ophiolite Classification and the Search for Archean Oceanic Crust. Lithos 100 (1–4), 14–48. https://doi.org/10.1016/j.lithos.2007.06.016.

Petrographic Code of Russia: Magmatic, Metamorphic, Metasomatic and Impact Formations, 2009. VSEGEI Publishing House, Saint Petersburg, 200 p. (in Russian) [Петрографический кодекс России. Магматические, метаморфические, метасоматические, импактные образования. СПб.: Изд-во ВСЕГЕИ, 2009. 200 с.].

Polyansky O.P., Semenov A.N., Vladimirov V.G., Karmysheva I.V., Vladimirov A.G., Yakovlev V.A., 2017. Numerical Simulation of Magma Mingling (Case of Bayankol Gabbro-Granite Series, Sangilen, Tuva). Geodynamics & Tectonophysics 8 (2), 385–403 (in Russian) [Полянский О.П., Семенов А.Н., Владимиров В.Г., Кармышева И.В., Владимиров А.Г., Яковлев В.А. Численная модель магматического минглинга (на примере баянкольской габбро-гранитной серии, Сангилен, Тува) // Геодинамика и тектонофизика. 2017. Т. 8. № 2. С. 385–403]. https://doi.org/10.5800/GT-2017-8-2-0247.

Rosenberg C.L., Handy M.R., 2005. Experimental Deformation of Partially Melted Granite Revisited: Implications for the Continental Crust. Journal of Metamorphic Geology 23 (1), 19–28. https://doi.org/10.1111/j.1525-1314.2005.00555.x.

Rudnev S.N., Serov P.A., Kiseleva V.Yu., 2015. Vendian–Early Paleozoic Granitoid Magmatism in Eastern Tuva. Russian Geology and Geophysics 56 (9), 1232–1255. https://doi.org/10.1016/j.rgg.2015.08.002.

Slama J., Kosler J., Condon D.J., Crowley J.L., Gerdes A., Hanchar J.M., Horstwood M.S.A., Morris G.A. et al., 2008. Plešovice Zircon – A New Natural Reference Material for U-Pb and Hf Isotopic Microanalysis. Chemical Geology 249 (1–2), 1–35. https://doi.org/10.1016/j.chemgeo.2007.11.005.

Sugorakova A.M., 2017. A Role of Gabbroid Magmatism in Formation of the Kaakhem Magmatic Area (Eastern Tuva). In: Petrology of Igneous and Metamorphic Complexes. Proceedings of the IX All-Russia Petrographic Conference (November 28 – December 26, 2017). Vol. 9. Publishing House of CSTI, Tomsk, p. 395–398 (in Russian) [Сугоракова А.М. Роль габброидного магматизма в формировании Каахемского магматического ареала (Восточная Тува) // Петрология магматических и метаморфических комплексов: Материалы IX Всероссийской петрографической конференции (28 ноября – 2 декабря 2017 г.). Томск: ЦНТИ, 2017. Вып. 9. С. 395-398].

Sugorakova A.M., Khertek A.K., 2017. The New Data to the Question of the Age of Associations Kaakhem Magmatic Area (Eastern Tuva). Geosphere Research 3, 50–60 (in Russian) [Сугоракова А.М., Хертек А.К. Новые данные к вопросу о возрасте Каахемского магматического ареала (Восточная Тува) // Геосферные исследования. 2017. № 3. С. 50–60]. https://doi.org/10.17223/25421379/4/7.

Sugorakova A.M., Yarmolyuk V.V., Lebedev V.I., Lykhin D.A., 2011. Late Paleozoic Alkali–Granitic Magmatism of Tuva and Its Relation to Intraplate Activity within the Siberian Paleocontinent. Doklady Earth Sciences 439, 1070. https://doi.org/10.1134/S1028334X11080198.

Sylvester P.J., 1998. Post-Collisional Strongly Peraluminous Granites. Lithos 45 (1–4), 29–44. https://doi.org/10.1016/S0024-4937(98)00024-3.

Taylor S.R., McLennan S.M., 1985. The Continental Crust: Its Composition and Evolution. Blackwell, Oxford, 379 p.

Tsygankov A.A., 2014. Late Paleozoic Granitoids in Western Transbaikalia: Sequence of Formation, Sources of Magmas, and Geodynamics. Russian Geology and Geophysics 55 (2), 153–176. http://dx.doi.org/10.1016/j.rgg.2014.01.004.

Ubide T., Gale C., Larrea P., Arranz E., Lago M., Tierz P., 2014. The Relevance of Crystal Transfer to Magma Mixing: A Case Study in Composite Dykes from the Central Pyrenees. Journal of Petrology 55 (8), 1535–1559. https://doi.org/10.1093/petrology/egu033.

Vladimirov A.G., Kruk N.N., Khromykh S.V., Polyansky O.P., Chervov V.V., Vladimirov V.G., Travin A.V., Babin G.A., Kuibida M.L., Khomyakov V.D., 2008. Permian Magmatism and Lithospheric Deformation in the Altai Caused by Crustal and Mantle Thermal Processes. Russian Geology and Geophysics 49 (7), 468–479. https://doi.org/10.1016/j.rgg.2008.06.006.

Whalen J.B., Currie K.L., Chappell B.W., 1987. A-Type Granites: Geochemical Characteristics, Discrimination and Petrogenesis. Contribution to Mineralogy and Petrology 95, 407–419. https://doi.org/10.1007/BF00402202.

Xiao W., Huang B., Han Ch., Sun Sh., Li J., 2010. A Review of the Western Part of the Altaids: A Key to Understanding the Architecture of Accretionary Orogens. Gondwana Research 18 (2–3), 253–273. https://doi.org/10.1016/j.gr.2010.01.007.

Yarmolyuk V.V., Kovalenko V.I., 2003. Batholiths and Geodynamics of Batholith Formation in the Central Asian Fold Belt. Russian Geology and Geophysics 44 (12), 1260–1274.

Yarmolyuk V.V., Kovalenko V.I., Kuz'min M.I., 2000. North Asian Superplume Activity in the Phanerozoic: Magmatism and Geodynamics. Geotectonics 34 (5), 343–366.

Yarmolyuk V.V., Kozlovsky A.M., Savatenkov V.M., 2019. Gigantic Batholiths of Central Asia and a Role of Mantle Plumes in Their Formation from the Isotopic (Nd, Pb) and Geochemical Data. In: Large Ingenuous Provinces in the History of the Earth: Mantle Plumes, Supercontinents, Climate Changes, Metallogeny, Oil and Gas Formation, Terrestrial Planets. Abstract volume of the VII International Conference (August 28 – September 8, 2019). Publishing House of CSTI, Tomsk, p. 193–194 (in Russian) [Ярмолюк В.В.,

Козловский А.М., Саватенков В.М. Гигантские батолиты Центральной Азии и роль мантийных плюмов в их формировании: по результатам изотопных (Nd, Pb) и геохимических исследований // Крупные изверженные провинции в истории Земли: мантийные плюмы, суперконтиненты, климатические изменения, металлогения, формирование нефти и газа, планеты земной группы: Тезисы VII Международной конференции (28 августа – 8 сентября 2019 г.). Томск: ЦНТИ, 2019. С. 193–194].

Yarmolyuk V.V., Kuzmin M.I., 2011. Rifting and Silicic Large Igneous Provinces of the Late Paleozoic – Early Mesozoic in the Central Asia. Available from: http://www.largeigneousprovinces.org (Last Accessed June 15, 2021).

Yarmolyuk V.V., Kuzmin M.I., Kozlovsky A.M., 2013. Late Paleozoic – Early Mesozoic Within-Plate Magmatism in North Asia: Traps, Rifts, Giant Batholiths, and the Geodynamics of Thear Origin. Petrology 21, 101–126. https://doi.org/10.1134/S0869591113010062.

APPENDIX 1 / ПРИЛОЖЕНИЕ 1

Table 1.1. Contents of major (wt. %) trace and rare-earth (ppm) elements in the representative samples of the early and late mingling
Таблица 1.1. Содержания петрогенных оксидов (мас. %) и редких элементов (ppm) в породах раннего и позднего минглинга

Components	Early-mingling rocks														
	Salic rocks				Mafic rocks					Intermediate rocks					
	Average (n=8)	К463-1	К508-3	ШВ-7	Average (n=9)	К480	К485-4	К505-11	К507-1	Average (n=15)	К483-3	К485-2	К505-12	К508-2	К510-1
SiO_2	66.22±2.7	68.40	65.17	63.07	50.87±2.6	47.53	49.64	50.75	48.19	58.16±2.3	56.77	60.90	60.43	55.96	57.34
TiO_2	0.52±0.2	0.26	0.70	0.72	2.01±0.2	1.80	2.05	2.33	2.15	1.47±0.4	1.60	1.09	1.24	2.08	1.71
Al_2O_3	16.31±1.0	16.00	15.85	17.41	15.85±0.7	16.02	15.59	16.60	14.76	16.47±1.0	15.60	16.00	15.97	15.42	17.13
$Fe_2O_3^T$	3.52±0.9	2.81	4.02	4.30	10.82±1.2	12.56	10.82	11.74	11.69	7.29±1.1	8.20	6.71	6.63	8.93	8.40
MnO	0.09	0.05	0.05	0.13	0.15	0.16	0.15	0.16	0.16	0.13	0.14	0.09	0.11	0.17	0.14
MgO	0.48±0.3	0.17	0.97	0.60	5.48±1.5	7.83	6.14	3.55	7.80	2.34±0.6	3.97	2.34	2.65	2.69	2.09
CaO	1.12±0.6	0.80	2.17	1.14	6.89±0.5	7.05	7.47	6.44	7.40	4.48±0.8	5.72	3.90	4.12	5.14	4.18
Na_2O	5.07±0.6	4.96	3.98	5.51	3.88±0.6	3.25	3.51	4.14	2.91	4.63±0.5	4.48	4.79	4.51	4.07	5.03
K_2O	5.74±0.8	5.29	5.26	6.47	2.14±0.4	1.62	2.44	2.31	2.64	3.63±0.9	2.82	3.22	3.60	3.28	3.02
P_2O_5	0.12	0.04	0.22	0.16	0.64±0.1	0.61	0.66	0.72	0.59	0.55±0.2	0.40	0.31	0.31	0.86	0.55
LOI*	–	0.23	1.24	0.25	–	0.97	0.84	0.76	1.35	–	0.47	0.45	0.64	1.33	0.55
Total	–	99.02	99.63	99.75	–	99.39	99.30	99.49	99.63	–	100.17	99.79	100.21	99.93	98.74
Rb	–	109	76	33	–	33	64	55	69	–	80	76	76	78	470
Sr	–	65	520	102	–	855	793	650	661	–	508	484	472	658	41
Y	–	26	17.1	29	–	18.2	25	35	21	–	35	40	33	31	0.44
Zr	–	431	488	706	–	172	216	323	166	–	341	444	366	318	6.9
Nb	–	39.4	23.5	29	–	21.6	33.2	29.3	28.1	–	50.3	50.8	52.5	38.5	1.3
Cs	–	1.24	1.96	–	–	2.0	1.44	1.51	1.96	–	1.75	2.9	1.63	1.96	61
Ba	–	577	1132	587	–	437	546	606	497	–	454	556	613	722	32
La	–	38	32	48	–	25	32	38	25	–	43	54	47	46	45
Ce	–	81	63	137	–	54	67	81	54	–	91	109	94	97	93
Pr	–	8.8	6.7	13	–	6.9	8.2	10.3	6.6	–	10.4	12.3	10.4	11.4	11
Nd	–	31	25	55	–	29	33	42	28	–	40	45	39	46	8.7
Sm	–	5.5	5.1	9.9	–	5.4	7.6	9.0	6.3	–	8.8	9.2	8.3	9.9	1.0
Eu	–	1.01	1.62	1.9	–	1.74	2.1	2.5	2.0	–	1.74	1.62	1.65	2.5	5.9
Gd	–	4.7	3.7	8.9	–	5.0	6.2	8.1	5.8	–	7.2	7.9	6.7	8.1	1.2
Tb	–	0.76	0.52	1.2	–	0.67	0.84	1.20	0.81	–	1.07	1.19	0.98	1.05	5.3
Dy	–	4.4	3.0	6.9	–	3.5	4.4	6.3	4.1	–	6.2	6.5	5.7	5.9	3.1
Ho	–	0.86	0.58	1.3	–	0.62	0.88	1.29	0.80	–	1.30	1.34	1.16	1.08	2.8
Er	–	2.5	1.59	3.8	–	1.68	2.2	3.4	1.89	–	3.4	3.7	3.2	2.7	0.40
Tm	–	0.38	0.26	0.52	–	0.23	0.30	0.46	0.25	–	0.53	0.54	0.44	0.40	2.0
Yb	–	2.5	1.58	3.6	–	1.50	1.90	3.0	1.61	–	3.5	3.6	2.8	2.6	9.2
Lu	–	0.38	0.25	0.48	–	0.23	0.28	0.43	0.23	–	0.49	0.51	0.42	0.37	2.4
Hf	–	9.6	11.1	13	–	3.8	5.0	7.1	3.9	–	8.7	10.4	8.9	7.3	2.3
Ta	–	2.1	1.43	1.6	–	1.25	1.57	1.65	1.57	–	2.9	2.6	3.0	2.3	747
Th	–	9.1	10.8	6.7	–	2.7	3.5	4.7	3.1	–	7.3	7.7	5.8	7.5	401
U	–	1.44	2.2	0.93	–	0.86	1.30	1.43	1.41	–	2.3	3.5	2.2	2.1	42
La/Yb	–	10.31	13.65	9.11	–	11.20	11.46	8.47	10.65	–	8.32	10.12	11.35	11.97	10.89
Gd/Yb	–	1.53	1.86	2.01	–	2.67	2.63	2.16	2.89	–	1.66	1.78	1.94	2.50	2.00
Eu/Eu*	–	0.59	1.10	0.60	–	1.01	0.93	0.88	1.00	–	0.65	0.57	0.65	0.83	0.87

Table 1.1. (continued)
Таблица 1.1. (продолжение)

Components	Late-mingling rocks									
	Salic rocks						Mafic rocks			
	Average (n=15)	К467-2	К487-3	К481	ШВ9	ШВ12	Average (n=7)	К467-1	К487-1	К488-2
SiO_2	73.13±2.8	73.60	69.66	76.01	73.78	74.25	49.52±1.0	50.32	48.27	49.14
TiO_2	0.29±0.2	0.27	0.47	0.10	0.25	0.18	2.22±0.1	2.18	2.43	2.37
Al_2O_3	13.48±1.0	13.38	14.90	12.78	13.53	13.18	16.52±0.7	16.99	16.53	16.29
$Fe_2O_3^T$	2.40±0.8	2.03	3.22	1.13	1.87	2.08	11.06±0.6	10.84	12.06	11.67
MnO	0.05	0.03	0.05	0.01	0.04	0.04	0.17	0.18	0.17	0.16
MgO	0.37±0.3	0.30	0.71	0.07	0.34	0.17	4.99±1.1	4.32	5.22	4.59
CaO	1.01±0.6	0.98	1.86	0.94	1.23	0.25	7.35±0.4	7.23	7.63	7.40
Na_2O	3.92±0.5	3.20	4.04	3.08	3.31	4.84	4.21±0.4	4.68	4.02	4.03
K_2O	4.69±0.3	5.32	4.38	5.11	4.93	4.57	2.01±0.1	1.77	1.97	2.02
P_2O_5	0.08±0.1	0.06	0.16	0.02	0.06	0.03	0.79±0.1	0.78	0.92	0.97
LOI*	–	0.06	0.45	0.54	0.31	0.26	–	0.44	0.86	0.76
Total	–	99.23	99.92	99.79	99.65	99.85	–	99.74	100.07	99.40
Rb	–	109	94	54	66	70	–	72	85	48
Sr	–	248	364	21	398	24	–	678	977	894
Y	–	10.7	18.7	0.16	7.3	16	–	26	23	24
Zr	–	209	266	3.0	151	323	–	285	200	225
Nb	–	18.4	26.1	0.97	4.9	23	–	35.3	27.7	26.0
Cs	–	1.52	1.48	106	–	–	–	3.2	1.63	1.15
Ba	–	659	909	12	1052	284	–	356	579	735
La	–	48	46	26	38	26	–	42	37	37
Ce	–	85	91	54	77	63	–	87	78	81
Pr	–	7.2	8.9	6.0	6.6	6.8	–	11.1	9.8	10.0
Nd	–	21	31	3.9	23	27	–	40	41	42
Sm	–	2.8	5.7	0.44	3.2	4.6	–	8.0	8.8	9.3
Eu	–	0.60	1.14	2.2	0.83	0.69	–	2.2	2.6	2.6
Gd	–	2.3	4.6	0.40	2.7	4.1	–	6.9	7.0	6.9
Tb	–	0.29	0.63	23	0.29	0.57	–	0.93	0.88	0.94
Dy	–	1.60	3.2	1.00	1.6	3.6	–	4.8	4.6	4.6
Ho	–	0.34	0.62	1.0	0.30	0.71	–	0.92	0.85	0.85
Er	–	1.05	1.63	0.16	0.98	2.2	–	2.6	2.2	2.1
Tm	–	0.18	0.25	1.6	0.14	0.35	–	0.35	0.28	0.27
Yb	–	1.23	1.65	3.0	1.1	2.8	–	2.2	1.71	1.69
Lu	–	0.19	0.25	2.7	0.16	0.38	–	0.31	0.24	0.24
Hf	–	5.3	6.6	0.46	4.1	8.1	–	5.9	4.5	5.1
Ta	–	1.34	2.3	137	0.49	2.4	–	1.73	1.16	1.30
Th	–	18.3	12.4	76	10.0	15	–	3.8	2.4	2.5
U	–	1.42	1.74	28	1.2	2.0	–	2.1	1.08	1.04
La/Yb	–	26.31	18.87	16.92	23.89	6.47	–	13.15	14.42	14.75
Gd/Yb	–	1.48	2.23	2.34	2.00	1.19	–	2.60	3.28	3.28
Eu/Eu*	–	0.70	0.66	0.39	0.85	0.48	–	0.88	0.97	0.96

Table 1.2. U-Pb zircon isotope ratios and derived age determinations from the early- and late-mingling rocks
Таблица 1.2. Результаты U-Pb изотопных исследований цирконов из пород раннего и позднего минглинга

Sample K 467-2 (late-mingling granosyenite)										
№	Isotope ratios				Rho	Age, Ma				D, %
	$^{207}Pb/^{235}U$	1s%	$^{206}Pb/^{238}U$	1s%		$^{206}Pb/^{238}U$	2s abs	$^{207}Pb/^{235}U$	2s abs	
1	0.31793	3.4	0.04441	2.0	0.58	280	11	280	19	99.27
2	0.31900	3.6	0.04456	2.0	0.55	281	11	281	20	99.60
3	0.32092	3.7	0.04482	2.0	0.54	283	11	283	21	100.18
4	0.32465	3.5	0.04535	2.0	0.55	286	11	286	20	101.32
5	0.32754	3.5	0.04575	2.0	0.57	288	11	288	20	102.21
6	0.31790	3.4	0.04450	2.0	0.58	281	11	280	19	101.27
7	0.32051	3.3	0.04477	2.0	0.60	282	11	282	18	100.06
8	0.32608	3.3	0.04565	2.0	0.61	288	11	287	19	103.93
9	0.32138	3.6	0.04489	2.0	0.55	283	11	283	20	100.33
10	0.31962	3.4	0.04464	2.0	0.59	282	11	282	19	99.79
11	0.31729	3.5	0.04432	2.0	0.56	280	11	280	20	99.07
12	0.32488	3.5	0.04538	2.0	0.56	286	11	286	20	101.39
13	0.32147	4.0	0.04490	2.0	0.51	283	12	283	22	100.35
14	0.32080	3.3	0.04529	2.0	0.60	286	11	283	19	110.85
15	0.31705	3.6	0.04428	2.0	0.56	279	11	280	20	99.00
16	0.32347	4.2	0.04547	2.1	0.49	287	12	285	24	107.15
17	0.32504	3.4	0.04540	2.0	0.59	286	11	286	19	101.44
18	0.32561	3.5	0.04551	2.0	0.58	287	12	286	20	102.24
19	0.32055	3.4	0.04477	2.0	0.59	282	11	282	19	100.07
20	0.31888	5.1	0.04454	2.1	0.41	281	12	281	29	99.56
21	0.32237	4.4	0.04503	2.1	0.47	284	12	284	25	100.63
22	0.32208	3.9	0.04507	2.0	0.52	284	12	284	22	102.26
23	0.32384	3.3	0.04523	2.0	0.60	285	11	285	19	101.08
24	0.31693	4.8	0.04427	2.1	0.44	279	12	280	27	98.96
25	0.32347	3.8	0.04518	2.0	0.53	285	12	285	22	100.96
26	0.32245	4.7	0.04504	2.1	0.44	284	12	284	27	100.65
27	0.32235	3.8	0.04580	2.0	0.54	289	12	284	21	118.84
28	0.31807	3.9	0.04443	2.0	0.52	280	11	280	22	99.31
29	0.32111	3.4	0.04485	2.0	0.59	283	11	283	19	100.24
30	0.31887	3.7	0.04480	2.0	0.55	282	12	281	21	105.13
31	0.32331	3.7	0.04516	2.0	0.55	285	12	285	21	100.91
32	0.31919	3.5	0.04458	2.0	0.58	281	11	281	20	99.66
33	0.32126	4.4	0.04487	2.1	0.47	283	12	283	25	100.29
34	0.31997	4.0	0.04469	2.1	0.52	282	12	282	22	99.89
35	0.31851	3.3	0.04449	2.0	0.60	281	11	281	19	99.45
36	0.32461	3.4	0.04571	2.0	0.59	288	12	286	19	109.34
37	0.32075	3.6	0.04480	2.0	0.56	282	11	283	21	100.13
38	0.34281	3.3	0.04788	2.0	0.60	301	12	299	20	106.86
39	0.31837	3.5	0.04447	2.0	0.57	280	11	281	20	99.41
40	0.32141	4.1	0.04489	2.0	0.50	283	12	283	23	100.33
41	0.32033	3.7	0.04474	2.0	0.55	282	11	282	21	100.01
42	0.32252	3.9	0.04505	2.1	0.52	284	12	284	22	100.67
43	0.32038	3.6	0.04475	2.0	0.57	282	11	282	20	100.02

Table 1.2. (continued)
Таблица 1.2. (продолжение)

№	Isotope ratios				Rho	Age, Ma				D, %
	$^{207}Pb/^{235}U$	1s%	$^{206}Pb/^{238}U$	1s%		$^{206}Pb/^{238}U$	2s abs	$^{207}Pb/^{235}U$	2s abs	
44	0.31952	4.6	0.04463	2.1	0.45	281	12	282	26	99.76
45	0.32244	4.3	0.04504	2.1	0.49	284	12	284	24	100.65
46	0.32219	4.2	0.04500	2.1	0.50	284	12	284	24	100.57
47	0.32387	3.2	0.04524	2.0	0.63	285	12	285	18	101.16
48	0.32156	3.8	0.04491	2.1	0.54	283	12	283	22	100.38
49	0.32109	3.5	0.04491	2.1	0.58	283	12	283	20	101.50
50	0.32409	3.4	0.04527	2.0	0.60	285	12	285	20	101.15
Sample K 484-1 (early-mingling monzodiorite)										
1	0,32976	2.5	0.04583	1.8	0.74	289	10	289	12	0.17
2	0.33239	2.7	0.04591	1.9	0.69	289	11	291	14	0.69
3	0.33274	1.9	0.04591	1.8	0.94	289	10	292	10	0.79
4	0.34371	1.9	0.04733	1.8	0.92	298	10	300	10	0.64
5	0.33912	2.3	0.04711	1.8	0.78	297	11	297	12	–0.10
6	0.33784	3.1	0.04691	1.9	0.61	296	11	296	16	0.00
7	0.33389	2.2	0.04652	1.8	0.83	293	10	293	11	–0.20
8	0.32842	2.6	0.04547	1.8	0.70	287	10	288	13	0.59
9	0.32668	2.0	0.04557	1.8	0.87	287	10	287	10	–0.10